Universitetet i Stavanger

DET TEKNISK-NATURVITENSKAPELIGE FAKULTET

BACHELOROPPGAVE

Studieprogram/spesialisering: Biologisk kjemi - bioteknologi - bachelorstudium i biologisk kjemi	Vårsemesteret, 2021 Åpen / Konfidensiell
Forfatter: Lene Victoria Bø	
Fagansvarlig: Peter Ruoff (UiS: Heinz Peter Ruoff) Veileder(e): Peter Ruoff & Qaiser Waheed	
Tittel på bachelorpppgaven: Dopaminregulert DOPA homeostase og nevrodegenerative forstyrrelser Engelsk tittel: Dopamine Regulated DOPA Homeostasis and Neurodegenative Disorders	
Studiepoeng: 20 stp	
Emneord: robust homeostasis, dopamine, DOPA, parkinson's disorder	Sidetall: total = 56 (eks denne siden) + vedlegg/annet: vedlegg er inkludert i total Stavanger, 12/05-21 dato/år

Forside for bacheloroppgaven
Det Teknisk-naturvitenskapelige fakultet

UNIVERSITY OF STAVANGER

Dopamine Regulated DOPA Homeostasis and Neurodegenative Disorders

by

Lene Victoria Bø

Bachelor Thesis in Biological Chemistry and Biotechnology

submitted to the
Faculty of Science and Technology
Department of Biology, Chemistry and Environmental Engineering

May 2021

"Q: Explain the concept of homeostasis?
A: It is when you stay at home all day and don't go out."

- Richard Benson, F in Exams: The Best Test Paper Blunders

UNIVERSITY OF STAVANGER

Abstract

Faculty of Science and Technology
Department of Biology, Chemistry and Environmental Engineering

Bachelor Thesis in Biological Chemistry and Biotechnology

by Lene Victoria Bø

Well-functioning homeostatic mechanisms lead to a robust homeostatic dopaminergic system. The dysfunction of this system is known to be associated with neurodegenerative disorders like Parkinson's disease (PD). In this examination of a robust homeostasis, dopamine (DA) is examined by its functionality of the gentle balance between synthesis, release, storage, re-uptake, and metabolism, as well as its role as a negative feedback regulator of dihydroxyphenylalanine (DOPA). In the computations I focus on the control DA has of the regulated species in the pathway, as well as demonstrating the impact of DOPA as a medication of PD.

Acknowledgements

I would like to thank Peter Ruoff for his training and help, as well as his caring and supportive advice. Additionally, I want to thank Qaiser Waheed in giving insight and further understanding. They both have provided programs to run the computations and assisted the modification of the programs by need.

Contents

List of Figures

Dedicated to my supportive parents, who have always pushed me to do my very best.

Chapter 1

Introduction

1.1 The Concept of Homeostasis

The ability to keep a specific component under given limits, is named *homeostasis* in physiology[2]. Physiology is a branch in biology, this branch has been organized into functions[3] of organisms as incorporated structures of cells, tissues, organs, and molecules or as the study of the nature of a healthy individual body, with all its functions[4].

To explain *homeostasis* further, Cannon stated that the term *homeostasis* should derive from the abbreviated form of *homoio* meaning *similar* instead of the Greek word for *same* which is *homo*. This emphasis allows for some variation of the state in the given body, whereas the steady state, according to mechanics, is produced by forces acting on the body, making the term *homeostatics* more correct use, since *stasis* means one stable state in equilibrium[5, 6]. This makes it a term which means the opposite, because the concept of *homeostasis* is that the states are constantly changing to achieve equilibrium, achieving it until the next change in forces.

Chemical forces need a feedback system to achieve *homeostasis*. Therefore, a control system is required to make *homeostasis* work, working to maintain a variable, like body temperature, at a given set point. The changes in the variable below or above the set point, makes a stimulus which is detected by a sensor, generating a response, which makes the variable go back to the set point. The response is often adjusted by the feedback system either negatively or positively, inhibiting or magnifying the stimulus, respectively. The negative feedback system is the major role player in homeostasis, while the positive one, anticipatory, not so much[7, 8]. Most organisms, like *Homo sapiens*, have a steady body temperature where the usual set point for humans is at 37°C[9].

This does not mean that the temperature is static at that point, because actions like breathing, eating, and laying down, stimulate the temperature by affecting organs and the nervous system to decrease or raise the temperature. This in turn creates a reaction, like when one freezes, the body starts to shake to mechanically raise the temperature, returning the temperature to its set point.

Campbell et al. describes the changes in the *homeostasis* in animals by the circadian rhythm, where the hormone melatonin, secreted at night will be affected by the longer nights of winter, affecting the set point. Additionally, melatonin regulates the core body temperature rhythm, lowering the heart rate and the body temperature[7]. Brown further points out that the hormone is a darkness signal, providing a feedback to the oscillator. The hormone is affected not only by darkness, but also by lifestyle, like having free environmental time cues, diseases causing insomnia, night shifts or shifting work schedules, as well as jet lags caused by changing time zones[10]. Thus, melatonin affects the *homeostasis* of the animal, where various set points get adjusted by the negative or positive feedback systems, preparing the body to sleep.

1.2 Milieu Intérieur

The first to conceptualize the modern-day word *homeostasis*, was Claude Bernard. In 1879, he introduced the concept of *milieu intérieur*, describing that the outer parts of aerial animals do not come in direct contact with the particles in the atmosphere, because of the interior environment, *milieu intérieur*, enveloping the histological cells, separating them from the outer space[11]. Dr Marion Thomas however, points out that the French had another contributor, the professor of histology Robin, who had a theory of how life should be examined – at the molecular level. The parts of the organism produced by the interaction between themselves, making the fluid of the body a main locus of the exchanges of molecules between the anatomical elements, named *milieu de l'intérieur*[12].

Charles Philippe Robin's theory about *milieu de l'intérieur* was proposed a year before Bernard's ideas, published in the book *Treatise of Anatomical and Physiological Chemistry, Normal and Pathologic* in 1853, Robin discussed the relationship of the organisms surrounding environment with the organism itself[13]. This made most believe that Bernard took the term to describe his findings from 1854 until his death in 1878, where he was aiming the term to the understanding of the life's mechanisms, which are composed of two, infused parts, the environment, and the organism. Even if he used Robin's term, it was Bernard who made the most progress, starting from assuming the blood to be the only internal environment, to finding that the higher animals are

more complex. The blood must be the device of circulation of maintenance of molecular exchange, containing all substances essential for the preservation of life, because it is the environment which is the bridge between the exterior and the interior parts of an organism[13, 14].

Walter Cannon was the one who created the term *homeostasis* with the complexity of physiological responses, which described how the body is sustaining its steady state. He emphasized that explaining the bodily factors which conserve the steady state, cannot be done by simple mechanics, since the bodily functions are much more complex. Moreover, the steady state is achieved by the automatic responses in the body to the external disturbances, therefore Cannon proposed postulates concerning homeostatic regulation, published in 1926[15];

1. In an open system such as our bodies represent, compounded of unstable material and subjected continually to disturbing conditions, constancy is in itself evidence that agencies are acting, or ready to act, to maintain this constancy.
2. If a state remains steady it does so because any tendency towards change is automatically met by increased effectiveness of the factor or factors which resist change.
3. Any factor which operates to maintain a steady state by action in one direction does not also act at the same point in the opposite direction.
4. Homeostatic agents, antagonistic in one region of the body, may be cooperative in another region.
5. The regulating system which determines a homeostatic state may comprise a number of cooperating factors brought into action at the same time or successively.
6. When a factor is known which can shift a homeostatic state in one direction it is reasonable to look for automatic control of that factor or for a factor or factors having an opposite effect[5, 15].

While Cannon has done much to explain *homeostasis* and its regulatory changes, it was Emerson who suggested that homeostatic effects are dynamic. In 1954, he explained that *homeostasis* is a sum composed of a web of effects with many feedbacks, both negative and anticipatory. These feedbacks make up small functions of *homeostasis* which interfere with each other, forcing them to coordinate into a well-functioning, but complex, organism[15].

In the following years, the term *homeostasis* has been studied further to understand the functions of the body. To understand the term, is to understand how one can battle

diseases. Diseases may occur when there is an impairment of normal bodily functions, where homeostatic imbalance may be the cause[16]. By constructing computer models, one can predict effects of manipulations of given variables which are regulated. It is the concepts of stress, allostatic load and allostasis which can be used as values, to construct the computer models[8].

1.3 Modeling robust homeostasis by integral control realized by zero-order kinetics

Computational biology systems, CBS, are divided into two separate parts: (i) simulation-based analysis, which exams hypotheses with *in silico* experiments; and (ii) knowledge discovery, which extracts patterns from vast numbers of experimental data, resulting in new hypothesis, which the simulation-based analysis can model[17]. By using mathematical representations of processes and components in biology, one can understand the responses expected for true organizing principles. Unfortunately, this is only true when the systems are of small size, since this mathematical analysis becomes too demanding for more extensive systems. The hypothesis although, is that these principles can be excepted to function[18].

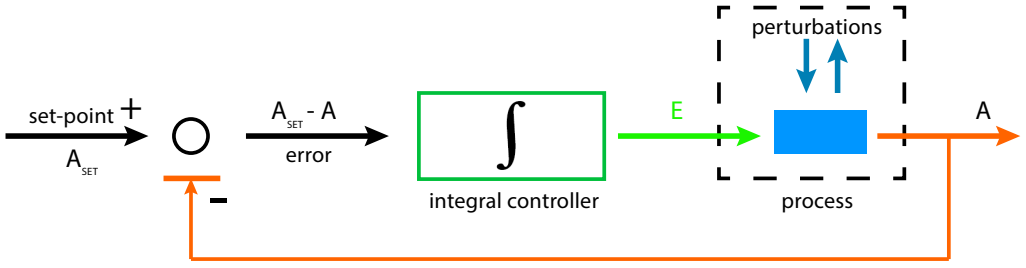

FIGURE 1.1: This figure shows the integral feedback control system, where the A_{set} is a set point which the concentration of A tries to reach by the integrate error, A_{set}-A. The product E is then subjected to perturbations, giving A, which both inhibits the flux of A and goes into another pathway. This continues until error becomes 0.[1].

Integral feedback control, as shown in Figure 1.1, involves the regulations of internal conditions at a constant level, *homeostasis*[19]. To illustrate the integral control strategy using CBS, as seen below in Figure 1.2, one can use the occurrence of zero-order kinetics in the processes[20], shown in Equation 1.2 below. Some of the control strategies are of enzyme inhibitions, which can be reversible, irreversible, and competitive, uncompetitive, and noncompetitive. The enzyme inhibitions can be defined mathematically with the Michaelis-Menten equation[21], which describes where the maximum

rate of an enzymatic reaction is reached when the concentration reaches 100% enzyme saturation[22].

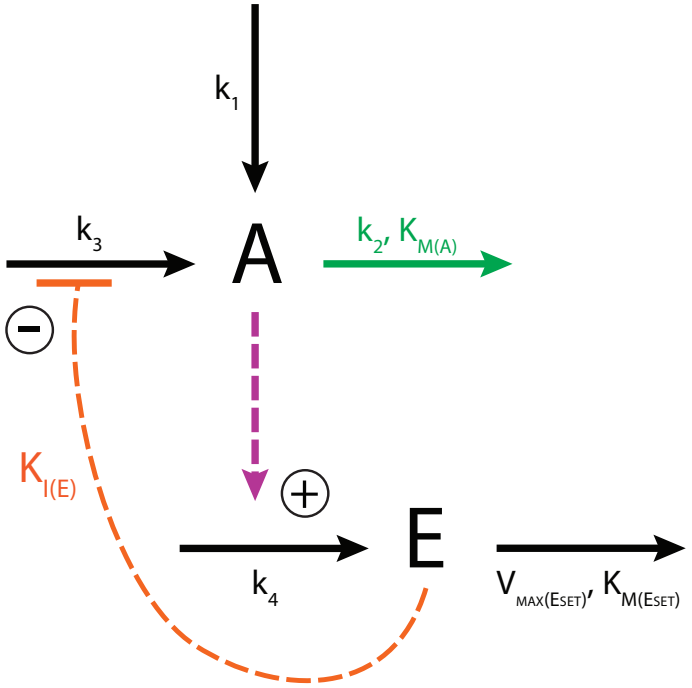

FIGURE 1.2: This figure shows the integral control of A, by E being the regulator of the regulated species A. There is a perturbation from A, indicated by green, into another pathway, and another pathway in violet which stimulates E. The inhibition of A is done by another other pathway, by $K_{I(E)}$, regulating the flux of k_3, regulating A[1].

Enzyme inhibition plays a role in how the neurotransmitter DA can be a potential mediating factor in a variety of neurogenerative disorders, such as schizophrenia, Parkinson's disease, and drug addiction[23]. The negative feedback control, illustrated in Figure 1.2, shows an inhibition, $K_I(E)$ of the enzyme depended by k_4, slowing down the production of A, because of the value of E, meaning that E is the regulator of the regulated species A. This is further explained by the following equations: Equation 1.1 and 1.2.

$$\dot{A} = k_1 + \overbrace{\frac{k_3 \cdot K_{I(E)}}{K_{I(E)} + E}}^{compensatory\ flux} - \frac{k_2 \cdot A}{K_{M(A)} + A} \tag{1.1}$$

$$\dot{E} = k_4 \cdot A - \frac{v_{max(ESET)} \cdot E}{K_{M(ESET)} + E}$$
$$if\ zero\ order \tag{1.2}$$
$$\dot{E}_{zero\ order} = k_4 \underbrace{(\frac{v_{max(ESET)}}{k_4} - A)}_{A_{set}}$$

The equations show the relationship the regulator has to its regulated species, whereas the over braced fraction in Equation 1.1 is the compensatory flux. This flux compensates for the fluctuations of the perpetuation k_1, but when the perpetuation is too large, the compensatory flux approaches its maximum value, making it equal to k_3. The underbraced A_{set} fraction in Equation 1.2 is describing that when E is in zero-order, it regulates A as shown in Figure 1.1.

1.4 Consequence of feedback dysfunction: Parkinson's disease

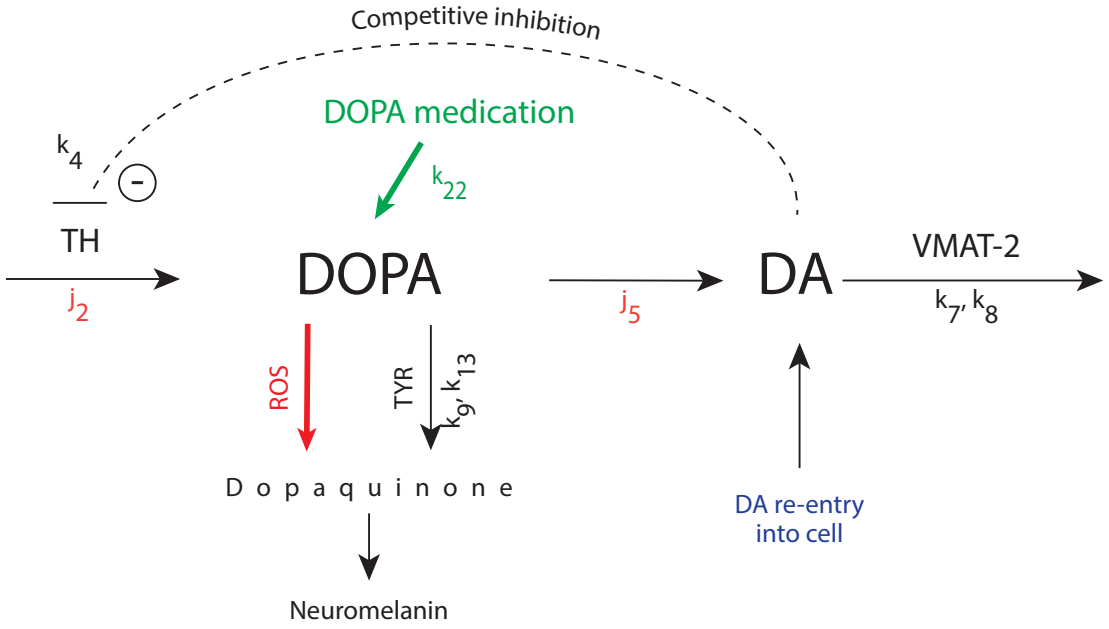

FIGURE 1.3: This model shows the production of DOPA, which lead to oxidization or a pathway into DA. DA controls the competitive inhibition of k_4, making this model based on the integral control shown in Figure 1.2 .

The neurogenerative disorder PD which is characterized by the loss of dopaminergic neurons[24, 25] which contain neuromelanin in the substantia nigra and are responsible for motor symptoms, like rigidity and speech deficits, of the disorder. As shown

in Figure 1.3, DOPA oxidation to DOPA o-quinone, along with aminochrome and 5,6-indolequinone, are one of the seemingly reasons for the neurodegenerative processes of PD, since they induce mitochondria and protein degradation dysfunction, like oxidative stress and formation of neurotoxic alpha synuclein protofibrils. These dysfunctions are the probable cause of PD having aging as its main risk factor. Yet, there is a protective system against DA oxidation in the cells, composed by DA re-uptake mediated by Vesicular Monoaminergic Transporter-2 (VMAT-2), neuromelanin formation, and two-electron reduction[26–30].The protective system slows down the formation of DOPA by inhibition, which can be explained by the following Figure 1.4.

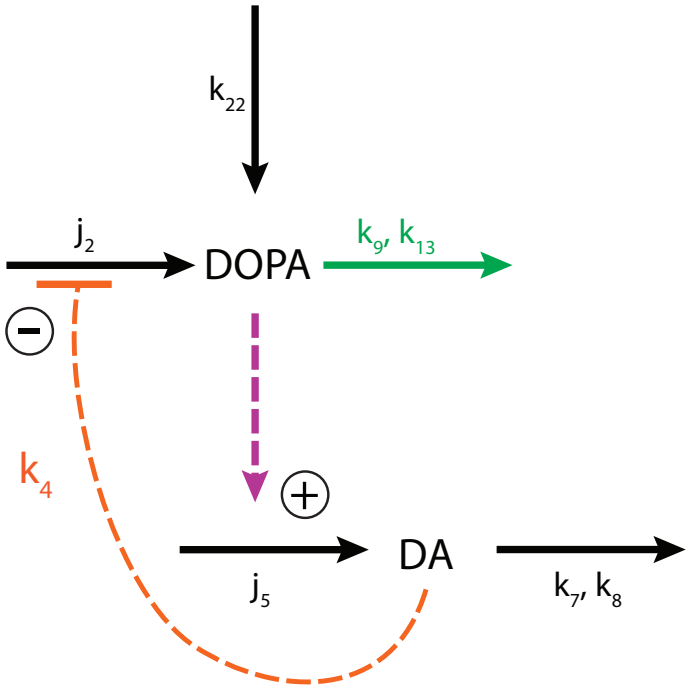

FIGURE 1.4: This negative feedback control is based on Figure 1.2, where A and E are replaced with DOPA and DA, respectively. The constants are replaced with constants and fluxes which are used in this thesis, where TH would be j_2 in this case. k_4 is the competitive inhibitor of TH.

In this case, A would be DOPA and E would be DA, where DA is the regulator, keeping DOPA under homeostatic control. Actually, Figure 1.4 may describe one of the potential targets of the catechol-containing precursor of DA, DOPA, which inactivate TH. TH is the rate-limiting enzyme of catecholamine synthesis, catalyzing the hydroxylation of Tyr to DOPA. Both DA and DOPA are capable of inactivating and covalently modifying TH, where they can kinetically inhibit the activity of TH by competitive inhibitors[31, 32].

1.5 The aim of thesis

The aim is to investigate the role of DA as a negative feedback regulator. That is, exploring how robust homeostasis is by regulating the values of fluxes and inhibitions of the pathway from Tyr to DA loading into vesicle(s). The role of DA will be investigated by complicating the first pathway, based on the Figures 1.3 and 1.4, and comparing them. The final goal is to identify the consequences of regulation, and how one can resolve the given complications medically.

Chapter 2

Materials and Methods

The modelling and computing were performed using Fortran subroutine LSODE[33] and PERL (www.perl.org). The figures were constructed by Adobe Illustrator (www.adobe.com), while the graphs were composed with gnuplot (www.gnuplot.info).

The models are labeled as Model x, where x being (a, b, ...). In addition, the runs have been named x-X, X being numbered to the run made, making it easier to find the given run. To simplify notation, the compounds are indicated as abbreviations found in Appendix A and the rate parameters are represented as kx's, where x=(1, 2, ...), regardless to their kinetic nature, whether they were Michaelis constants, turnover numbers, or inhibition constants.

The results are written as 3 significant figures, with some exceptions.

2.1 Solving rate equations by LSODE subroutine

Fortran subroutine LSODE solves nonstiff and stiff systems of differential equation[33]. By first providing a subroutine of a function f and its dimension, which supplies the vector function f by loading ydot(i) with f(i)[34]. After determining if the problem is stiff or not, the main program is made, where the vector f is defined, with a start and end time.

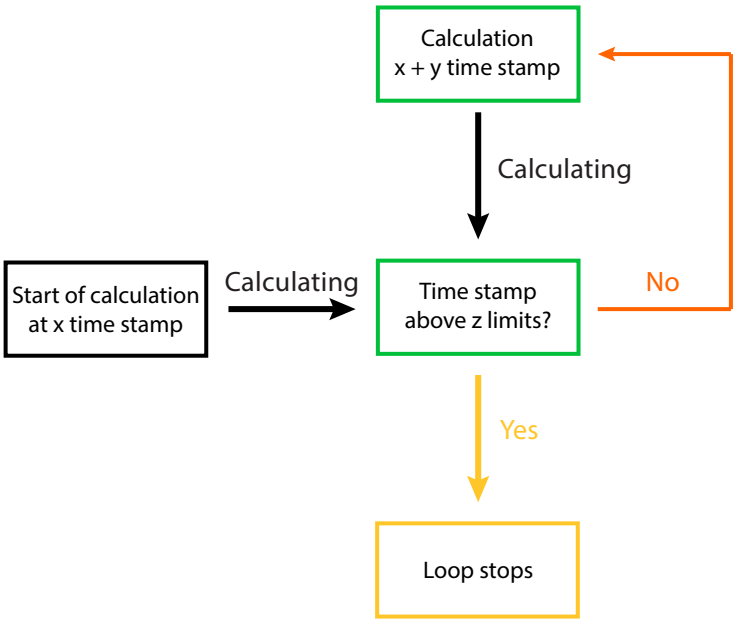

FIGURE 2.1: This figure shows the flow chart of LSODE subroutine with its given criteria of the loop. The criteria are *x, y, z*, in this case *0 min, x+1 min, 5000 min* for first phase.

As shown in Figure 2.1, the loop has been given a start time and an end time, with criteria of the loop. The loop starts at the given time, 0 min, checking if the result is below or equal given limits, if affirmative, then the loop continues. If the result at one timestamp check is above the limits, then the loops stops, and the summary is written out as PERL is run to encode graphs, producing them with gnuplot[35].

2.2 The values of the rate parameters *kx* and their reference

The values found in their respected references are listed underneath. These values are used to compute the models found in Appendix B. The ones without citation, have been decided to be very small or 0 to have a model without much disruption of the rate parameter in question.

rate parameter	value	citation	comment
k_1	5.00μM/min	[36]	phase 1
k_1	6.00μM/min	[36]	phase 2
k_1	20.0μM/min	[36]	phase 3
k_2	$200min^{-1}$	[37, 38]	N/A
k_3	74.4μM	[39]	N/A
k_4	45.0μM	[36, 40]	N/A
k_5	3.10μM/min	[41, 42]	N/A
k_6	346μM	[41, 42]	N/A
k_7	1.50μM	[43, 44]	N/A
k_8	0.29μM/min	[43, 44]	N/A
k_9	2.30μM/min	[45]	N/A
k_{10}	$0.25min^{-1}$	no citation	chosen
k_{11}	1.00μM/min	[46, 47]	N/A
k_{12}	50.0μM	[37]	N/A
k_{13}	437μM	[45, 48]	N/A
k_{14}	$0min^{-1}$	no citation	for Models *a, b, c*
k_{14}	$500min^{-1}$	[46]	for Model *d*
k_{15}	2.30μM/min	[45]	N/A
k_{16}	50.0μM	[49]	N/A
k_{17}	0.01μM/min	[46]	N/A
k_{18}	$1.00 \times 10^5\mu$M/min	[46]	N/A
k_{19}	100μM	no citation	chosen
k_{20}	0.10μM	[46]	N/A
k_{21}	1.00×10^{-4} μM	[46]	N/A
k_{22}	0μM/min	no citation	chosen

2.3 Time intervals for phases

phase	start time	end time	time interval
1^{st}	0.00 min	4999 min	$[0, 5000\rangle$
2^{nd}	5000 min	9 999 min	$\langle 5000, 10000\rangle$
3^{rd}	10 000 min	15 000 min	$\langle 10000, 15000]$

Chapter 3

Results and Discussion

3.1 Model *a*: Changing the constants of maximum rate and Michaelis-Menten constants

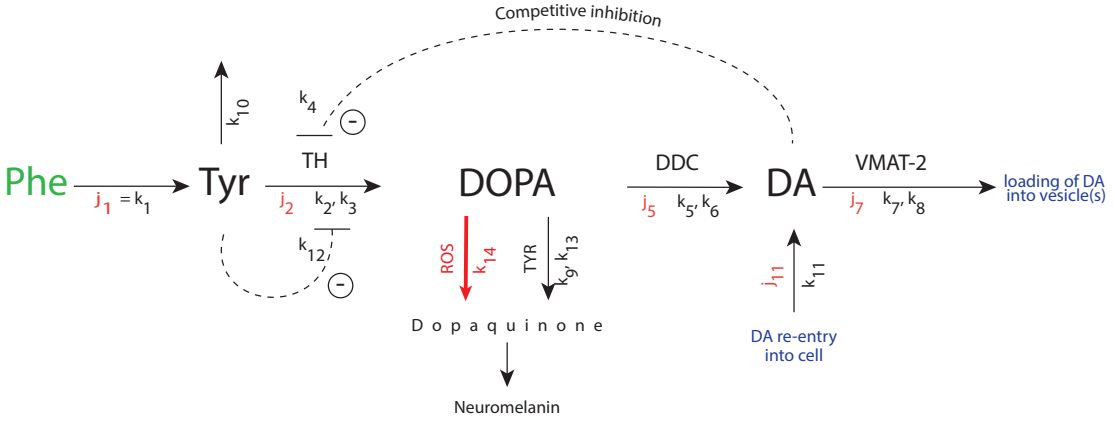

FIGURE 3.1: The Model *a*, show the different fluxes, j_1 to j_{11}, maximum velocity constants, V_{max}, Michaelis-Menten-constants, K_M, and other properties and outcomes. First the j_1 flux introduces L-tyrosine (Tyr) from Phenylalanine (Phe) in green. Tyr has two pathways: a perturbation by k_{10}, and another pathway catalyzed by tyrosine hydroxylase (TH), producing DOPA, with the help of k_2 and k_3, being V_{max} and K_M, respectively. Thereafter, DOPA can turn into Dopaquinone, making Neuromelanin, by reactive oxygen species (ROS) or by being catalyzed by tyrosinase (TYR). DOPA may turn into DA, via catalysis with DOPA decarboxylase (DDC). DA is catalyzed by vesicular monoaminergic transporter-2 (VMAT-2), and loaded into vesicles(s). Additionally, there are two competitive inhibitions, one depended on k_4 and DA, while the second is depended on Tyr and k_{12}, both inhibiting TH. The concentration of DA is additionally depended on k_{11}, which is the re-entry of DA.

The rate equations for Tyr, DOPA, and DA are:

$$\frac{d(Tyr)}{dt} = k_1 - \frac{k_2 \cdot Tyr}{k_3\left(1 + \frac{DA}{k_4}\right) + Tyr} \cdot \frac{k_{12}}{k_{12} + Tyr} - k_{10} Tyr \tag{3.1}$$

$$\frac{d(DOPA)}{dt} = \frac{k_2 \cdot Tyr}{k_3\left(1+\frac{DA}{k_4}\right)+Tyr} \cdot \frac{k_{12}}{k_{12}+Tyr} - \frac{k_9 \cdot DOPA}{k_{13}+DOPA} - \frac{k_5 \cdot DOPA}{k_6+DOPA} - k_{14}DOPA \tag{3.2}$$

$$\frac{d(DA)}{dt} = k_{11} + \frac{k_5 \cdot DOPA}{k_6+DOPA} - \frac{k_7 \cdot DA}{k_8+DA} \tag{3.3}$$

With these rate equations, Equations 3.1, 3.2 and 3.3, are describing what happens to the concentrations of Tyr, DOPA and DA. k_{11} is a rate constant which affects DA by increasing the concentration by re-entry, thereby increasing the inhibition, k_4, of TH. The increase of k_{11} will decrease the concentration of DOPA. The set point of DOPA is given by Equation 3.4 below.

$$DOPA_{set} = \frac{k_6(k_7 - k_{11})}{k_5 + k_{11} - k_7} \tag{3.4}$$

The constant k_1, as shown as the first constant in Figure 3.1, seem to regulate the conversion of Phe to Tyr, the j_1 flux dependent on k_1. This conversion has been studied and it was found to be lower in end-stage renal disease (ESRD) patients than in the control group, showing a difference of 40% during the postabsorptive state and the amino acid replacement. Proposed treatment is to supply Tyr to patients with ESRD[50]. There has been found an increased risk of PD in ESRD patients, with a higher relative risk for women and younger patients with ESRD compared to the control group[51].

3.1.1 Investigating k_1 effect on Tyr concentration

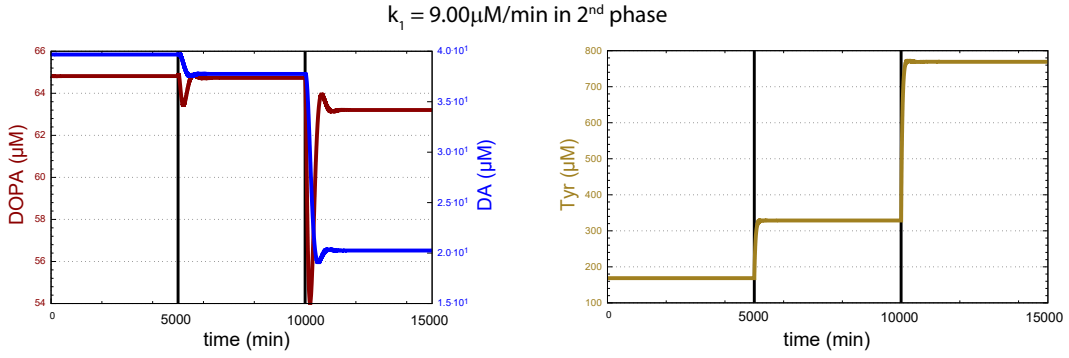

FIGURE 3.2: Run *a*-07 has k_1 changed from 6.00μM/min in the second phase to 9.00μM/min. The final concentrations of Tyr, DOPA and DA are 329μM, 64.7μM and 37.8μM, respectively.

When changing the constants one by one, from the values found in Section 2.2 and Appendix B.1, to check how well the homeostasis may vary without destabilizing, several interesting values were found. If k_1 is a enzymatic reaction, not a zero-order as in Model *a*-*d*, Lazar et al. account that k_1 values is in dependence of the enzyme's phosphorylation status. When the enzyme is in non-phosphorylated form the pH is at 7.0 and k_1=6μM/min, while in phosphorylated form it has a k_1 of 45.0μM/min[36]. For instance, when changing the k_1 value of 6.00μM/min to a lower value, the trend was less Tyr. Subsequently, lowering the concentration of the later products and inhibition factors. When using the value of 45.0μM/min, the time needed to reach homeostatic set value for DOPA is long in contrast to a lower value of k_1. After k_1 was enlarged, the production of the latter went up, but did not exceed too much from the standard from Appendix B.1. When k_1 was enlarged by 50%, to 9.00μM/min, the concentration of Tyr ended up as 329μM, as seen in Figure 3.2. The final concentration is 3.32 times higher than the highest normal Tyr concentration of 99.0μM[52]. Interestingly, the abnormally high concentration does not crash the homeostasis, even in the model of Appendix B.1 being of 762μM, meaning that when the enzyme is phosphorylated and the production exceeds its maximum flux of 45.0μM/min, the system manages to overwrite this and therefore not crashing the homeostasis. Although, it seems unlikely that this would happen, because of the limits of TH.

The possible reason for the nonserious consequences of k_1 is that the j_1 flux might contain a steady stream of Tyr which comes from protein-containing foods[53]. Even if the value of k_1 is decreased by 50% from the original value from Appendix B.1, giving the final concentration of 88.6μM, it is still in the normal state for nonfasting condition in healthy young adults. The plasma Tyr concentrations should vary between 61.0μM and 99.0μM[52]. This indicates either a strong homeostatic response, or a computing too easy-going on the lowering of the rate constant.

What could happen in the long term, is a buildup of Tyr in the tissues and organs, leading to tyrosinemia-like symptoms, and if the abnormal concentration of Tyr continues it may lead to an eventual death[54]. Luckily, by this model and the second phase shortness, the final concentration did not reach 500μM, which is the minimum value of Tyr concentration for Tyrosinemia type 2, but it is not far from Tyrosinemia type 3 minimum value of 350μM. The conditions could lead to intellectual disabilities, skin or ocular changes[**?**].

3.1.2 Regulating the first-order elimination of Tyr by changing k_{10}

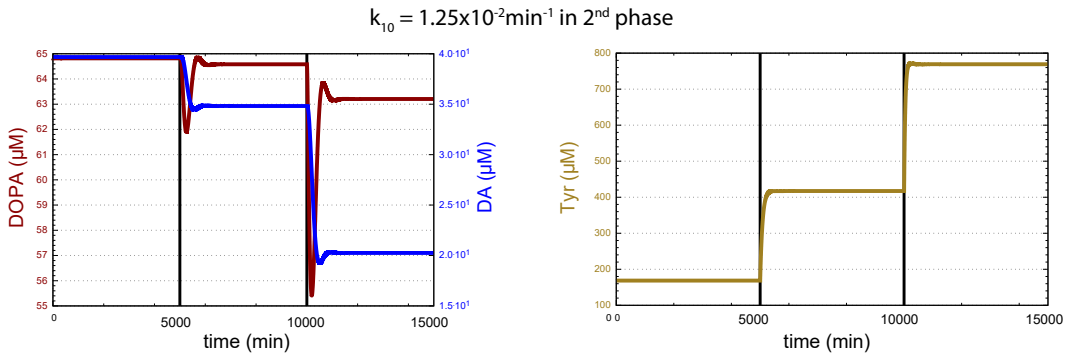

FIGURE 3.3: Run a-56 shows the graphs when k_{10} is changed from $0.25min^{-1}$ in the second phase to $1.25\times10^{-2}min^{-1}$. The final concentrations of Tyr, DOPA and DA are 417μM, 64.6μM and 34.8μM, respectively.

Another explanation of the abnormally high Tyr and why the homeostasis stays intact, is the non-specific, first order removal of Tyr, depended on the value of k_{10}. A first-order elimination is a constant proportion, like a percentage, of substance eliminated per unit of time[22]. Because k_{10} is depended on the size of Tyr, the higher the concentration is, the more Tyr is removed. In fact, if this first order constant is too high of value, like $3.75\times10^{-2}min^{-1}$ as seen in Figure 3.3, the set point of DA drops in the second phase, but if the value of k_{10} is lowered in the third phase to $1.25\times10^{-2}min^{-1}$, DOPA drops in its set point. Tyr on the other hand, is affected greatly, having a higher concentration when the constant is lowered, and contradictory when the constant value is raised. The explanation may be that the higher the value, the higher the fluxes which lower DA, while the lower it is, the more DA is made, decreasing DOPA. As described by the rate equations 3.3 and 3.2.

To put k_{10} in a medical perspective, the first-order elimination might regulate the decarboxylation of Tyr into Tyramine (TA)[56], which may be the reason for the high Tyr not affecting DOPA and DA too much, when k_1 was too large of value. TA is a compound that produces peripheral cardiovascular effects, especially if ingested or in high accumulation, and if accumulated along with monoamine oxidase inhibitors (MAO-I), it can precipitate a hypertensive crisis, because it inhibits monoamine oxidase to break down TA. When the hypertensive crisis escalades into a hypertensive emergency once there is end-organ damage such as papilledema, retinal hemorrhages, intracranial bleeds, acute renal failure, or pulmonary edema[57, 58]. Monoamine oxidase-B inhibitors (MAO-B) are a class of medications which are used to treat symptoms of PD, since they reduce the motor fluctuations. They work by hindering the breakdown of neurotransmitters, like DA[59]. This breakdown of DA, as seen when increasing the value of k_{10}, is most likely

because of monoamine oxidase. Meaning that if a patient with the homeostasis of an highly increased k_{10}, should lower their intake of TA by ingestion, and start medication with MAO-I.

3.1.3 Exploring K_M kinetics by changing k_3

In the Model a in Figure 3.1, there are constants which are Michaelis-Menten constants, which follow the Michaelis-Menten kinetics, described by the Michaelis-Menten equation shown underneath by Equation 3.5:

$$v = \frac{\mathrm{d}[P]}{\mathrm{d}t} = V_{max}\frac{[S]}{K_M + [S]} \tag{3.5}$$

Equation 3.5 is a description of reaction rate r, making [P] the rate of formation of product, and [S] of substrate. V_{max} is the maximum rate achieved by the system, happening at saturating substrate concentration.

These kinetics are based upon the general description of the velocity and gross mechanism of enzyme-catalyzed reactions. These assume that the rapid reversible formation of a complex between a substrate and an enzyme, as well as assuming that the rate of formation of the product is proportionate to the concentration of the complex. The velocity of such reactions is the greatest when all the active sites are filled with substrate[60]. The Michaelis-Menten constant, K_M, is defined as the substrate concentration at which the reaction rate is half of its maximal value, meaning half of the active sites are occupied. In general, indicating the affinity of an enzyme for a given substrate. The lower the value, the higher affinity[61], thus affecting the stability of the Enzyme-Substrate Complex.

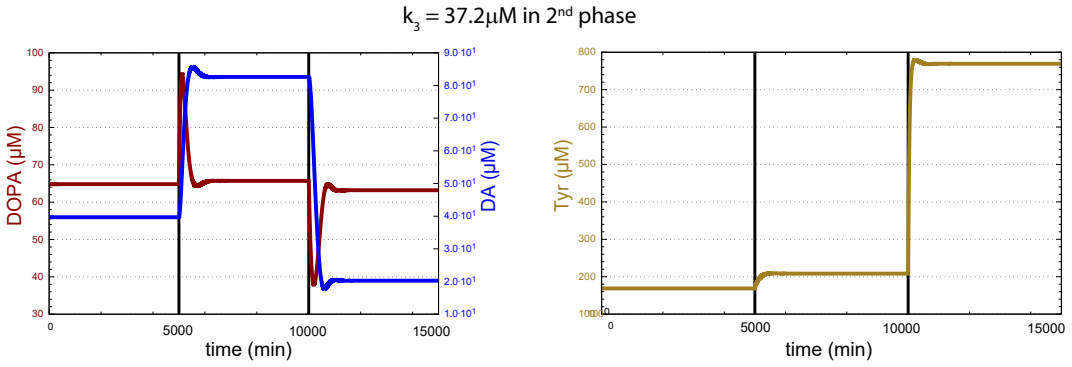

FIGURE 3.4: Run a-14 has k_3 changed from 74.4μM in the second phase to 37.2μM. The final concentrations of Tyr, DOPA and DA are 208μM, 65.7μM and 82.6μM, respectively.

As for k_3, a Michaelis-Menten constant, the results in Figure 3.4 show that the lower the value is, lowest at 37.2μM, the less concentration of both DOPA and DA, while Tyr was quite unaffected by both lower and higher values from earlier set point, with highest being 112μM. According to the kinetic theory of Michaelis-Menten, the rate of an enzymatic reaction would increase as the substrate concentration increases, since the other constants are not changing simultaneously with the k_3, then the DOPA lowers its set point from the previous one given in Appendix B.1, affecting DA concurrently. Therefore, the higher this Michaelis-Menten-constant is, the more DOPA and DA accumulates, as seen when the k_3 was increased. Sura et al. report that TH isoforms K_I values for DA are in the range of 4 to 7.41μM for the phosphorylated enzyme, while the range is 3.17 to 4.52μM for the unphosphorylated one[40]. When running the value of 4.00μM, the response time of the controller is much lower, affecting mostly DOPA and DA, as stated.

Hence, when Yildiz et al. immobilized TH with electrodes, where they found that an substantial decrease in the K_M value leads to the tendency of an enzyme to bind its substrate more sternly than the free enzyme and CP-*co*-PPy/tyrosinase electrode do, henceforth, the Enzyme-Substrate Complex stays together for a long time, which makes the enzymatic reaction rate of PEO-*co*-PPy/tyrosinase electrode the slowest[62]. In comparison to the results of k_3, the finds are similar, when the K_M constant decreases, the accumulation of DOPA and DA decreases accordingly, because of the Enzyme-Substrate Complex stays longer together.

3.1.4 Challenging the regulating properties of DA by changing k_{11}

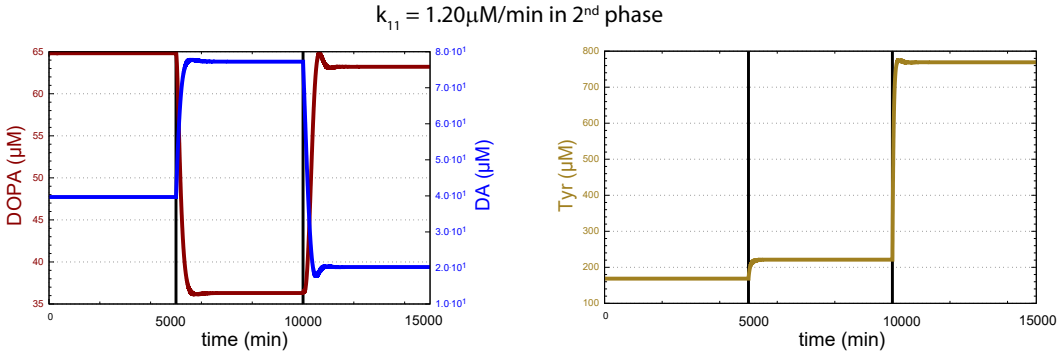

FIGURE 3.5: The output of run *a*-66 when the rate constant of k_{11} is changed from 1.0μM/min in the second phase to 1.20μM/min. The final concentrations of Tyr, DOPA and DA are 221μM, 36.3μM and 77.0μM, respectively. The changes shown in the graphs of DOPA and DA to the left, and the Tyr concentrations against time in minutes shown in the graph at the right.

k_{11} is a rate constant describing the re-uptake of DA into the nerve cell, from the outside of the system, by dopaminergic transporters. During the modelling of this constant, Tyr, DOPA, and DA were affected by the value of this inflow. Figure 3.5 shows that even though it is a re-entry of DA, the concentration of Tyr and DOPA get higher. The higher the inflow of DA, because of a higher valued k_{11}, the higher the concentrations of DA. According to Equation 3.2 and 3.3, the concentrations are affected by each-other, confirming the decrease of the DOPA concentration when the DA concentration goes up, because of increase in k_{11}.

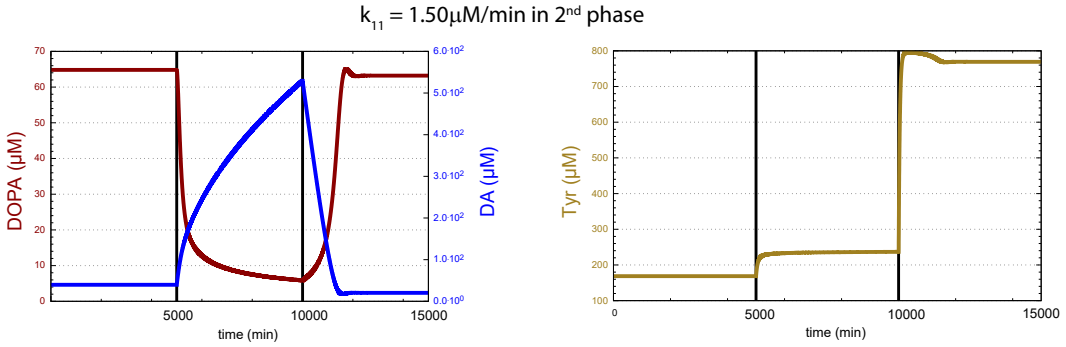

FIGURE 3.6: The run a-67 of Model a, when the maximum rate constant k_{11} is increased from 1.20μM/min, as in Figure 3.5, to 1.50μM/min in the second phase. The resulting concentrations of Tyr, DOPA and DA are 238μM, 5.85μM and 529μM, respectively.

Actually, when the k_{11} is too high, like in Figure 3.6, the homeostasis clearly breaks. The concentration of DA rapidly increases into a breakdown, without the time needed to recover until the next, third phase. DOPA, in contrast, drops in concentration, indicating that the high concentration of DA lowers the needed production of DOPA. Since the DA rate of VMAT-2, k_7 and k_8, is not changed, not letting the accumulating DA out, then inhibitors like k_4 must inhibit TH, to limit the production of DOPA. This limitation does not occur in Figure 3.6, because k_4 is a constant of 4.00μM, a value taken from the Sura et al. range of 4.00-7.41μM[40].

3.2 Model *b*: Comparing the latter results with a model with an additional TH pathway

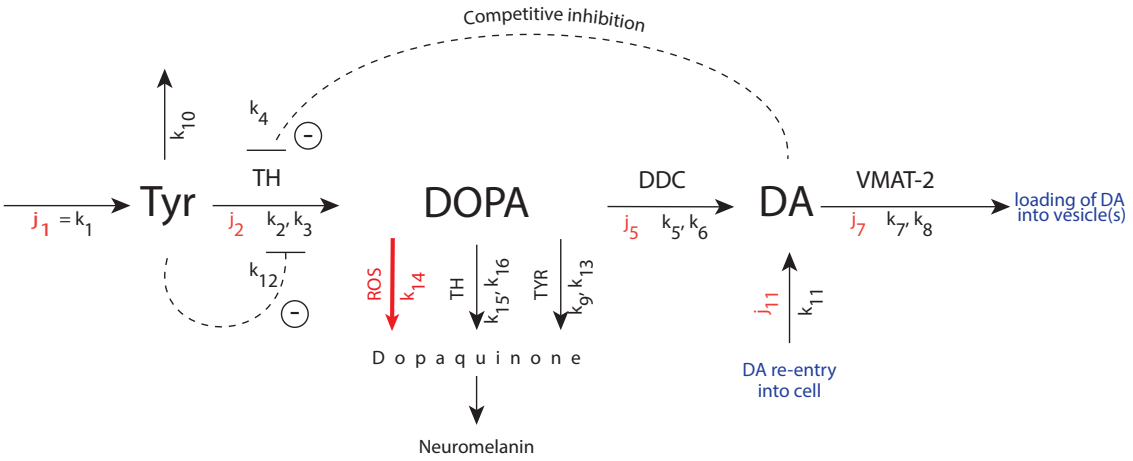

FIGURE 3.7: Model *b* shows the fluxes, constants and the outcomes of the given reactions, just as in the Model *a* in Figure 3.1. In this model, Phe is excluded for simplification, and two constants have been added, k_{15} and k_{16}, being V_{max} and K_M respectively. These control the catalyzation of DOPA by TH into Dopaquinone, meaning that TH now has a bigger role in Model *b* than in Model *a*.

The rate equations for Tyr, DOPA, and DA are:

$$\frac{d(Tyr)}{dt} = k_1 - \frac{k_2 \cdot Tyr}{k_3\left(1+\frac{DA}{k_4}\right)\cdot\left(1+\frac{DOPA}{k_{16}}\right)+Tyr} \cdot\left(\frac{k_{12}}{k_{12}+Tyr}\right) - k_{10}Tyr \tag{3.6}$$

$$\frac{d(DOPA)}{dt} = \frac{k_2 \cdot Tyr}{k_3\left(1+\frac{DA}{k_4}\right)\cdot\left(1+\frac{DOPA}{k_{16}}\right)+Tyr}\cdot\left(\frac{k_{12}}{k_{12}+Tyr}\right) - \frac{k_9 \cdot DOPA}{k_{13}+DOPA} - \frac{k_5 \cdot DOPA}{k_6+DOPA} - k_{14}DOPA - \frac{k_{15}\cdot DOPA}{k_{16}\left(1+\frac{Tyr}{k_3}\right)+DOPA} \tag{3.7}$$

$$\frac{d(DA)}{dt} = k_{11} + \frac{k_5 \cdot DOPA}{k_6+DOPA} - \frac{k_7 \cdot DA}{k_8+DA} \tag{3.8}$$

$DOPA_{set}$ equation is:

$$DOPA_{set} = \frac{k_6(k_7-k_{11})}{k_5+k_{11}-k_7} \tag{3.9}$$

To check the mechanisms of homeostasis, another pathway was added to the Model *a*, to make another scheme, Model *b*, as seen in Figure 3.7. The enzyme TH catalyzes two pathways in this model, resulting in competitive inhibition between the two pathways. The values of the additional pathway are based on Haavik reports of them being 2.3μM/min for k_{15} and k_{16} being 50μM[49]. According to Roskoski competitive inhibitors, in this case TH, are structural equivalents of the substrate whose concentration differs, resulting in an unchanged V_{max}. K_M although, increases with an increasing inhibitor concentration[63], described with the following equation, Equation 3.10:

$$v_0 = \frac{V_{max}[S]}{K_M(1 + \frac{[I]}{K_I}) + [S]} \tag{3.10}$$

Following the theory above, then the results should increase the concentration of Tyr and DA, while lowering the DOPA concentration. Essentially, the result should amplify the former results in Model *a* of Figure 3.1. The results are compared with the results of Model *a*, keeping in mind the Model *b* without any changes made, found in Appendix B.2.

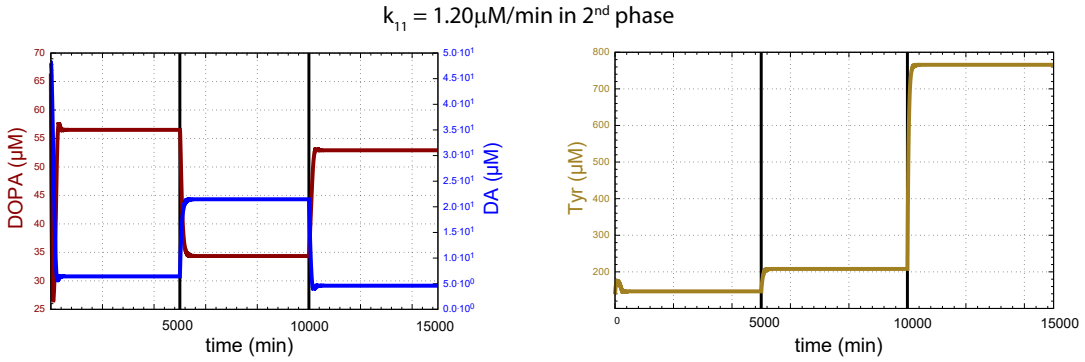

FIGURE 3.8: Run *b*-66 has the same k_{11} value in the second phase as in Figure B.2. This model has an addition of k_{15} and k_{16} constants. They are constant and unaltered from the model in Appendix B.2, having 2.3μM/min and 50μM, correspondingly, through all phases. The resulting concentrations of the second phase are 208μM, 34.4μM, and 21.5μM for Tyr, DOPA and DA, respectively.

Comparing the finds in Figure 3.8, with an increased k_{11} in the second phase, against the results in Figure 3.5, the Tyr levels actually stay similar in the second phase, but change in the third phase compared to the Model *a*, as seen in Table 3.1. In fact, this behavior was anticipated, but the main difference between the two finds, was the concentrations of DA and DOPA. DOPA does not accumulate as much as in Figure 3.5, while DA increases, meaning that the addition of oxidation of DOPA by Tyr, has a great effect in maintaining homeostasis.

	Model a		Model b	
Run	a-66	a-67	b-66	b-67
Tyr (μM)	221	237	208	236
DOPA (μM)	36.3	5.85	34.4	4.32
DA (μM)	77.3	529	21.5	366

TABLE 3.1: Displays the final concentrations of second phase from the runs 66 and 67 for both Model a and b, whereas run x-66 has k_{11}=1.20μM/min while k_{11} of x-67 is 1.50μM/min.

Indeed, when the extracellular DA is increased because of an overexpression of TH, the inhibition of TH increases by auto receptors[47], as seen in Table 3.1 where Tyr concentration is decreases from Run 66 to 67, which is resulting in less DOPA compared to Figure B.1 and B.2 in Appendix B.1 and B.2. Challenging this is the Tyr concentration, which is grander when k_{11} is increased, leading to further exploration of this with the Model c, Section 3.3, where the inhibiting auto receptors are included. This may be a result of the addition of Tyr oxidation, as well.

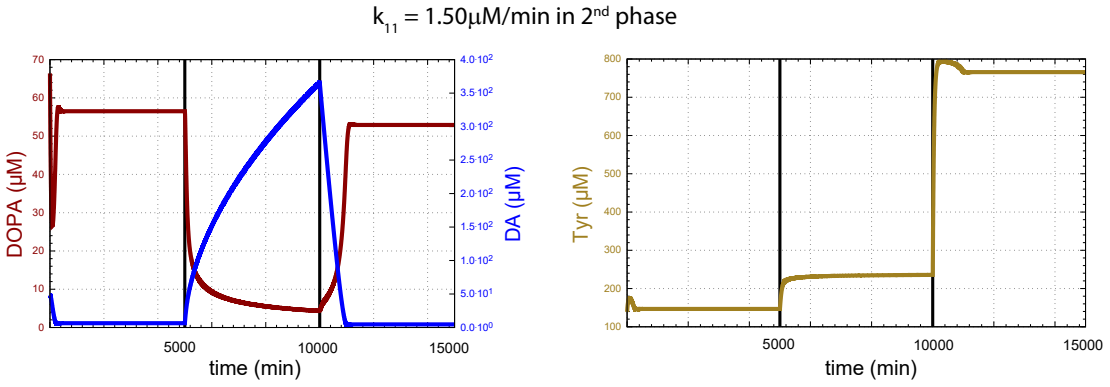

FIGURE 3.9: This run b-67 is similar to run b-66 in Figure 3.8, but with a k_{11} value of 1.50μM/min. Running the file, resulted in the three graphs, discussed in the text, and the concentrations 236μM for Tyr, 4.32μM for DOPA, and 366μM for DA at the end of the second phase.

Interestingly, the results in Figure 3.9 are not as different to Figure 3.6, as Figure 3.8 was to Figure 3.5 in the last section. When k_{11} is too high in phase 2, the DA increases rapidly in both models, with a dropping DOPA concentration and no significant difference in Tyr. In the model of Best et al., the cytosolic DA concentration is set to 2.65μM and DOPA to 0.36μM, at steady state[47]. Meaning that the concentration of 236μM for Tyr, 4.32μM for DOPA, resulted by a k_{11} of 1.50μM/min, is quite high from the given values of Best. Interestingly, Best et al. note the k_{11} flux to be of 80.1μM/h[47], being

1.36μM/min, contributing to why k_{11} of 1.20μM/min did not crash homeostasis, while the later k_{11} did.

The effect of the addition of k_{15} and k_{16} is shown when comparing Figure 3.8 to Figure 3.9, where the DA concentration is stabilizing quicker in the Model *b*, than in Model *a*. The study of Zhou et al. showed that the decarboxylation of 250μM DOPA has a slow increase of formation of DA over 240 min, including the 39.6% DOPA disappearance by enzymatic decarboxylation with enzyme concentration at $2.07\times10^{-3}1/min$[64]. If this decarboxylation is generalized into per enzymatic decarboxylation disappearance, even if the concentration is small, then it would certainly affect the final concentration of DA, if the removal by two enzymatic decarboxylation disappearances as in the Model *b* rather than the single one in Model *a*.

3.3 Model *c*: Addition of DA in synaptic cleft into the scheme, comparing with previous results

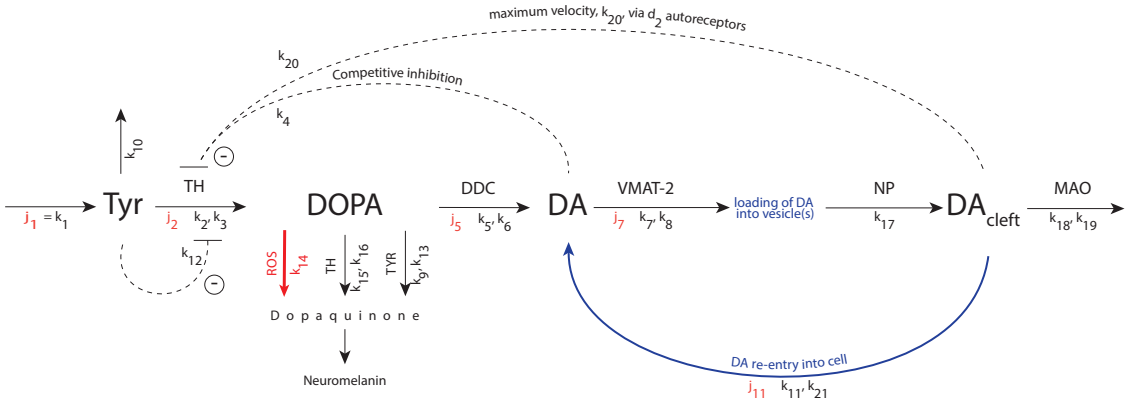

FIGURE 3.10: Model *c*, based on the previous Model *b* in Figure 3.7, is introducing the reactions after DA has been loaded into vesicle(s). It is a nerve pulse which releases the DA from the vesicle(s), which is depended by the flux k_{17}, asserting DA into DA_{cleft}. While DA is in the synaptic cleft, it may make DA re-enter into the cell by k_{11}, as seen in Model *a* and Model *b*, but making it more complicated by depending it on the concentration of DA_{cleft} and the Michaelis-Menten-constant k_{21}. DA_{cleft} may competitively inhibit TH via d_2 auto receptors, depending on the maximum velocity of k_{20} or DA_{cleft} can turn into MAO, driving the reaction forward by the V_{max} and K_M, which are the k_{18} and k_{19}, respectively.

The rate equations for Tyr, DOPA, DA, $DA_{vesicle}$, and DA_{ext} are:

$$\frac{d(Tyr)}{dt} = k_1 - \frac{k_2 \cdot Tyr}{k_3\left(1+\frac{DA}{k_4}\right)\cdot\left(1+\frac{DOPA}{k_{16}}\right)+Tyr} \cdot\left(\frac{k_{12}}{k_{12}+Tyr}\right) - k_{10}Tyr \tag{3.11}$$

$$\frac{d(DOPA)}{dt} = \frac{k_2 \cdot Tyr}{k_3\left(1+\frac{DA}{k_4}\right)\cdot\left(1+\frac{DOPA}{k_{16}}\right)+Tyr}\cdot\left(\frac{k_{12}}{k_{12}+Tyr}\right) - \frac{k_9 \cdot DOPA}{k_{13}+DOPA} - \frac{k_5 \cdot DOPA}{k_6+DOPA} - k_{14}DOPA - \frac{k_{15}\cdot DOPA}{k_{16}\left(1+\frac{Tyr}{k_3}\right)+DOPA} \tag{3.12}$$

$$\frac{d(DA)}{dt} = j_{11} + \frac{k_5 \cdot DOPA}{k_6+DOPA} - \frac{k_7 \cdot DA}{k_8+DA} \tag{3.13}$$

$$\frac{\mathrm{d}(DA_{vesicle})}{\mathrm{d}t} = \frac{k_7 DA}{k_8+DA} - k_{17}DA_{vesicle} \tag{3.14}$$

$$\frac{\mathrm{d}(DA_{ext})}{\mathrm{d}t} = k_{17}DA_{vesicle} - \frac{k_{18}DA_{ext}}{k_{19}+DA_{ext}} - \frac{k_{11}DA_{ext}}{k_{21}+DA_{ext}} \tag{3.15}$$

To test the robust homeostasis of the Model *b*, Figure 3.7, the Model *c* in Figure 3.10 has its "loading of DA into vesicle(s)" further stimulated by a nerve pulse into the synaptic cleft, leading into a catalyzation by MAO. Best et al. state the $DA_{vesicle}$ at 81μM at steady state, in their model, is being released into DA_{cleft} at 81μM/h[47]. Here, this would be the rate constant k_{11}, where the rate in the following Figure 3.11 is just below Best's 1.36μM/min.

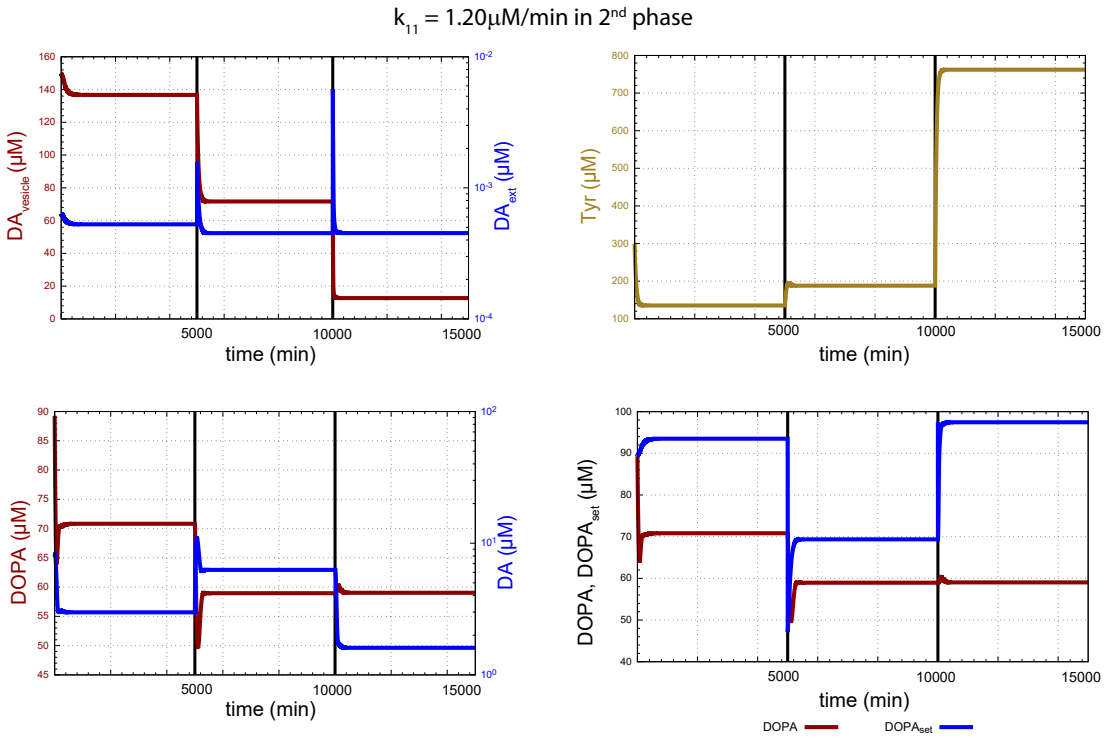

FIGURE 3.11: The output of run c-66 of Model c is shown here, and it is different from the output of models a and b, generating four graphs with $DA_{vesicle}$ and DA_{ext} plotted against time in minuets at the top-left, whereas the graph to the bottom-left illustrates the DOPA and DA found in the cell, plotted against time. The top-right graph displays Tyr, while the last graph show DOPA and the $DOPA_{set}$ against time. Here, the value of k_{11} is changed from 1.00μM/min, as in Figure B.3, to 1.20μM/min in the second phase. The concentrations at the end of phase 2 are 188μM, 59.0μM, 6.27μM, 71.7μM, and $4.51\times10^{-4}\mu$M for Tyr, DOPA, DA, $DA_{vesicle}$, and DA_{ext}, correspondingly.

	Runs with $k_{11} = 1.20\mu$M/min		
Run	a-66	b-66	c-66
Tyr (μM)	221	208	188
DOPA (μM)	36.3	34.4	59.0
DA (μM)	77.3	21.5	6.27
$DA_{vesicle}$ (μM)	N/A	N/A	71.7
DA_{ext} (μM)	N/A	N/A	4.51×10^{-4}

TABLE 3.2: Displays the final concentrations of second phase from the runs 66 for Model a, b, and c, where run THx-66 has k_{11}=1.20μM/min.

Figure 3.11 and Table 3.2 show that the addition of further pathways and inhibition by auto receptors, k_{20}, affect the scheme by giving more DOPA and DA_{total}, using more Tyr than in the latter Models a and b. In fact, this suggests that DA is the regulator

of DOPA, since the final concentrations from all three models depend on the amount of DA. Sura et al. reported that the considerable change in the affinity of an isoform of TH for DOPA upon phosphorylation, propose that the inhibition of the human enzyme by DOPA is not significant for regulation *in vivo*, whereas for inhibition by DA is. The concentration of DOPA in adrenal tissue and brain is rather low, due to its swift conversion to DA by DDC, suggesting that the unphosphorylated TH is not significantly inhibited by DOPA in the cell[40].

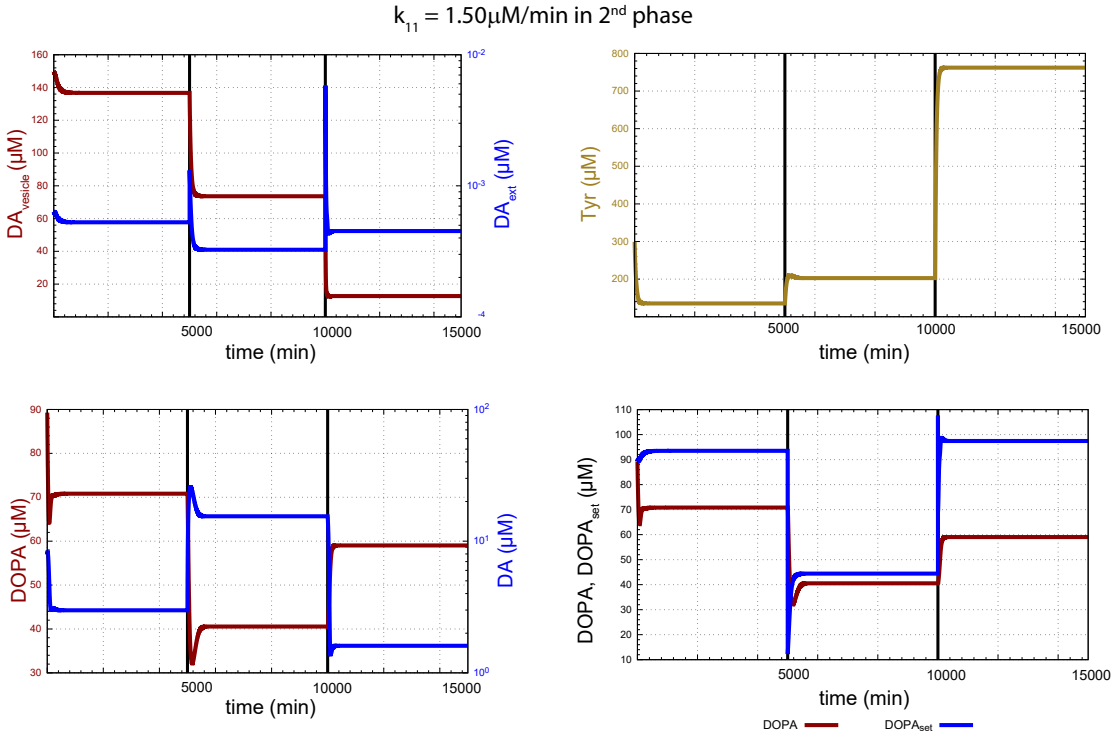

FIGURE 3.12: Run c-67 has a value of k_{11}, which is of 1.50μM/min in the second phase. The resulting concentrations of phase 2 are 178μM for Tyr, 71.8μM for DOPA, 3.19μM for DA, $DA_{vesicle}$ with 68.8μM, and 5.33$\times 10^{-4}\mu$M for DA_{ext}

	Runs with k_{11} = 1.50μM/min		
Run	a-67	b-67	c-67
Tyr (μM)	237	236	203
DOPA (μM)	5.85	4.32	40.6
DA (μM)	529	366	15.5
$DA_{vesicle}$ (μM)	N/A	N/A	73.6
DA_{ext} (μM)	N/A	N/A	3.25×10^{-4}

TABLE 3.3: Displays the final concentrations of second phase from the runs 67 for a, b, and c schemes, where run x-67 has k_{11}=1.50μM/min.

When k_{11} is over Best's 1.36μM/min estimation[47], the final concentrations of DA lower in all forms, listed in Table 3.3. All concentrations are lower than in the two previous schemes, as well as for c-66, but the concentration of DOPA, which increased rather much. This further confirms Sura et al. finds, when the re-entry of DA increases, the more DA tries to control the concentration of DA_{total}, by decreasing the set-point of DOPA, as seen when comparing the fourth graph in Figure 3.11 and 3.12. $DOPA_{set}$ is calculated by the following Equation 3.16:

$$DOPA_{set} = \frac{k_6(k_7 - j_{11})}{k_5 + j_{11} - k_7} \tag{3.16}$$

$$j_{11} = \frac{k_{11} \cdot DA_{cleft}}{k_{21} \cdot DA_{cleft}} \tag{3.17}$$

The Equation 3.17 is the velocity flux of the re-entry of DA from DA_{cleft}. This flux is heavily affecting $DOPA_{set}$, indicating that DA is the regulator of the set point of DOPA, as seen in Equation 3.16.

3.4 Model *d*: Medicating assumed Parkinson's disorder with DOPA

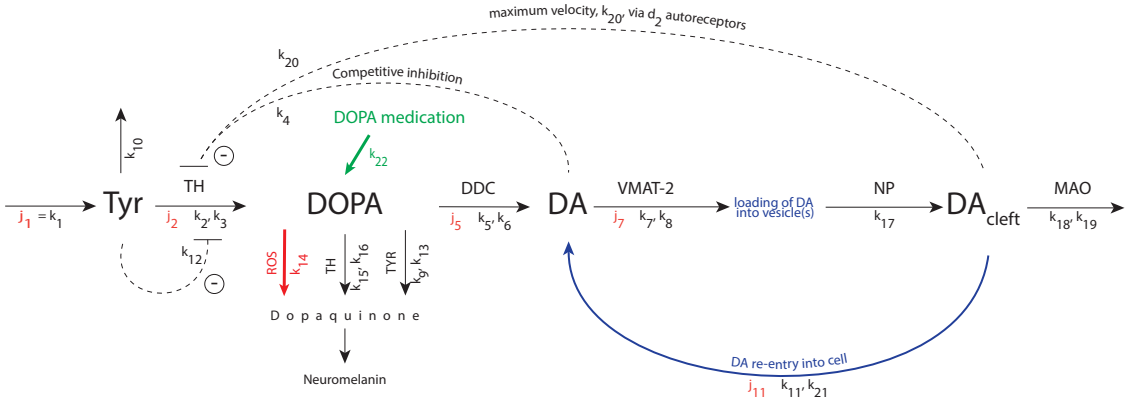

FIGURE 3.13: Model d, based on the previous Model c in Figure 3.10. Model d is introducing the medication, DOPA, into the model. The value k_{22} is a perpetuation, affecting mainly the concentration of DOPA, affecting the other concentrations. This perpetuation into DOPA is the computation of administration of medication.

The rate equations for Tyr, DOPA, DA, $DA_{vesicle}$, and DA_{ext} are:

$$\frac{d(Tyr)}{dt} = k_1 - \frac{k_2 \cdot Tyr}{k_3\left(1+\frac{DA}{k_4}\right)\cdot\left(1+\frac{DOPA}{k_{16}}\right)+Tyr}\cdot\left(\frac{k_{12}}{k_{12}+Tyr}\right) - k_{10}Tyr \tag{3.18}$$

$$\begin{aligned}\frac{d(DOPA)}{dt} &= k_{22} + \frac{k_2 \cdot Tyr}{k_3\left(1+\frac{DA}{k_4}\right)\cdot\left(1+\frac{DOPA}{k_{16}}\right)+Tyr}\cdot\left(\frac{k_{12}}{k_{12}+Tyr}\right) \\ &- \frac{k_9 \cdot DOPA}{k_{13}+DOPA} - \frac{k_5 \cdot DOPA}{k_6+DOPA} - k_{14}DOPA - \frac{k_{15}\cdot DOPA}{k_{16}\left(1+\frac{Tyr}{k_3}\right)+DOPA} + k_{22}\end{aligned} \tag{3.19}$$

$$\frac{d(DA)}{dt} = j_{11} + \frac{k_5 \cdot DOPA}{k_6+DOPA} - \frac{k_7 \cdot DA}{k_8+DA} \tag{3.20}$$

$$\frac{\mathrm{d}(DA_{vesicle})}{\mathrm{d}t} = \frac{k_7 DA}{k_8+DA} - k_{17}DA_{vesicle} \tag{3.21}$$

$$\frac{\mathrm{d}(DA_{ext})}{\mathrm{d}t} = k_{17}DA_{vesicle} - \frac{k_{18}DA_{ext}}{k_{19}+DA_{ext}} - \frac{k_{11}DA_{ext}}{k_{21}+DA_{ext}} \tag{3.22}$$

$DOPA_{set}$ equation is:

$$DOPA_{set} = \frac{k_6(k_7 - j_{11})}{k_5 + j_{11} - k_7} \tag{3.23}$$

Neuromelanin is only formed in neurons by catecholamine producing regions, becoming observable when a human is of 3 years, accumulating over time because of the lack of a degrading mechanisms[25]. TH has a potential to damage catecholaminergic neurons by contributing to the production of dopaquinones[65], which may lead to PD[66] because of accumulation of neuromelanin. PD is also characterized by the decrease in the concentration of DA[67]. Various concentrations of DA have been shown to be toxic to numerous cell types including striatal and cortical cells. The toxic effects are the production of reactive quinones by ROS, the oxidative DA metabolism[68]. To demonstrate this, Figure 3.12 in section 3.3, is used with a change of the ROS pathway dependent on k_{14}. The change is determined to be $500 min^{-1}$, because Segel reported that turnover numbers vary from 50.0 to $10.0^7 min^{-1}$[46].

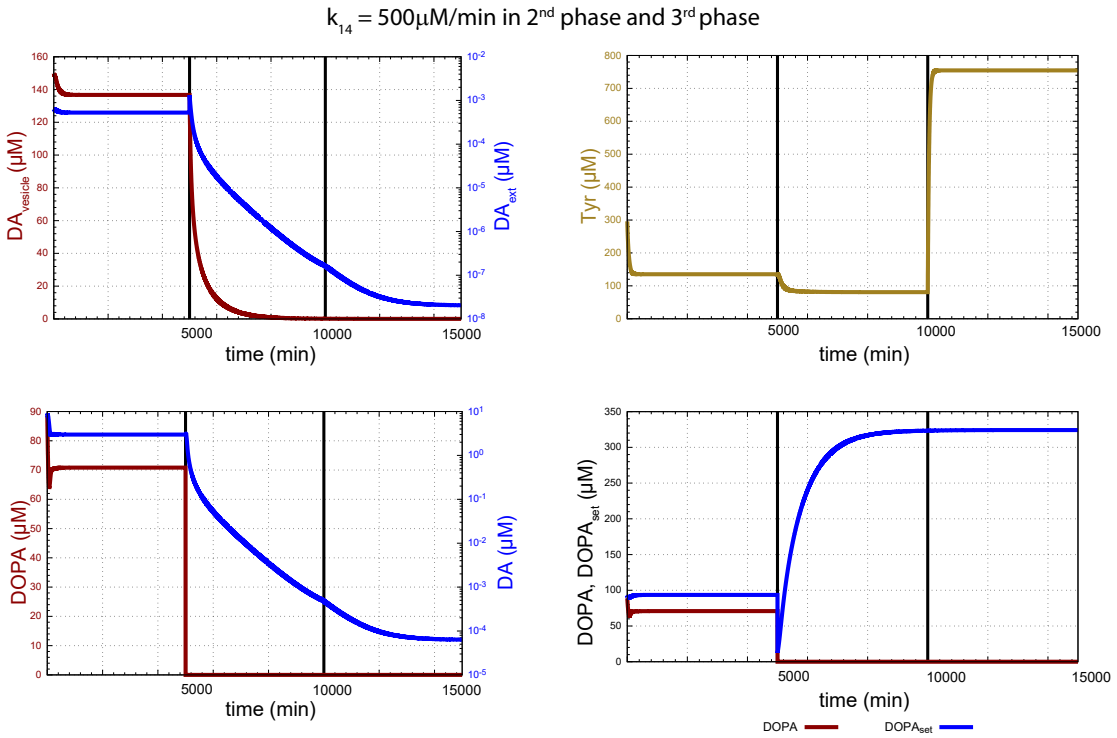

FIGURE 3.14: Run d-p1 has a value of k_{14}, which is of $500min^{-1}$ in the third phase. The resulting concentrations of phase 3 are 755μM for Tyr, $2.26\times10^{-3}\mu$M for DOPA, $6.35\times10^{-5}\mu$M for DA, $DA_{vesicle}$ with $1.64\times10^{-2}\mu$M, and $2.06\times10^{-8}\mu$M for DA_{ext}.

The finds in Figure 3.14 show a decrease in DA and DOPA, as well as an increasing in $DOPA_{set}$ when compared to Figure B.4 in Appendix B.4. The increase is quite large, most likely because of the increased oxidation of DOPA, therefore needing higher concentration of DOPA for robust homeostasis. Although the oxidation of DOPA to neuromelanin is a harmless and normal process, it is only when the individual has an intact neuromelanin-containing dopaminergic neurons[27]. Regrettably, since Greggio et al. found that TH enhances the toxicity in the presence of oxidative toxins like DA, leading to a reducing of the viability of these neurons[65].

To slow down this vicious cycle, there was introduced a pharmacological therapy of PD in 1967, where DOPA was a part of the medication[27]. Huot et al. had a study where they found the patients to have six times less TH+ neurons, treating them with 1-3,4-DOPA, to compensate for the loss of striatal DA[69]. Levodopa is a medication which is typically administered at 150-600 mg/day[70], where 300 mg should be the first dosage[71]. The Figure 3.14 is therefore adjusted with k_{22} being 1060μM/min in the second and third phase, with the result shown in Figure 3.15 underneath.

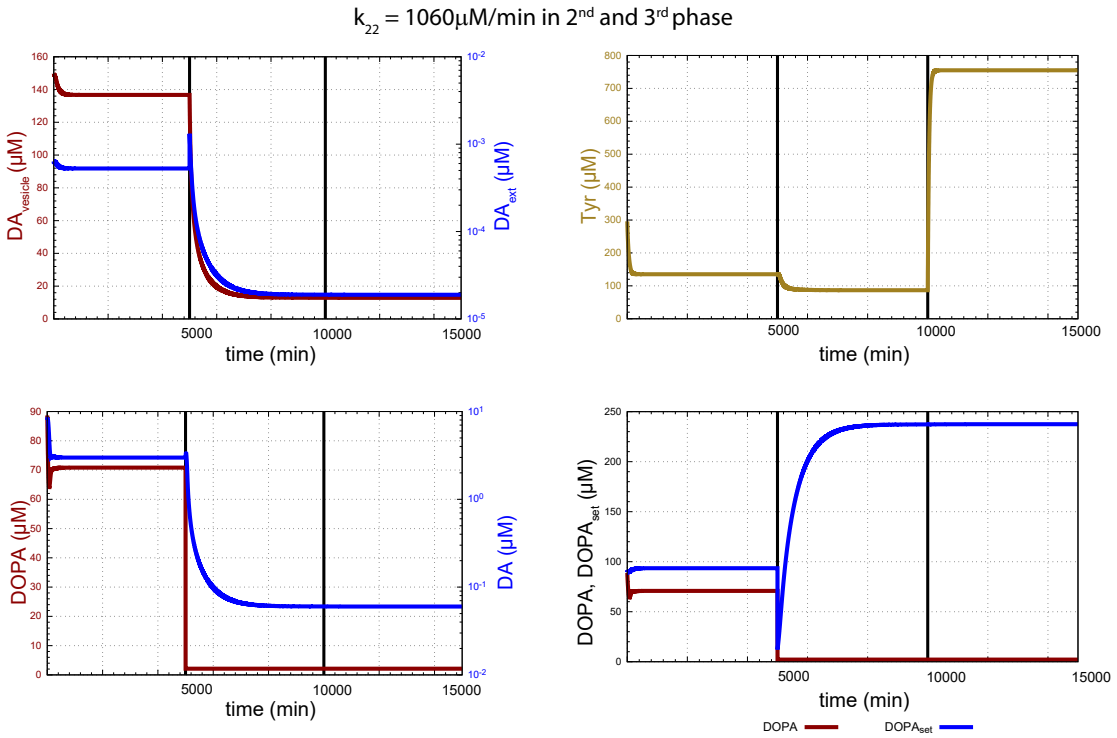

FIGURE 3.15: This run d-p2 is similar to the run d-p1 in Figure 3.14, but has a value of k_{22}, which is of 1060μM/min in the second and third phase. The resulting concentrations of phase 3 are 755μM for Tyr, 2.12μM for DOPA, $6.01\times10^{-2}\mu$M for DA, $DA_{vesicle}$ with 12.9μM, and $1.89\times10^{-5}\mu$M for DA_{ext}.

When the drug, DOPA medication, has been administered continuously by 300mg, as shown in Figure 3.15, the DOPA concentration increases, resulting in an increase of DA in all forms, when comparing the Figures 3.14 and 3.15. The set-point of DOPA also increases. Interestingly, there is a rather huge mismatch in $DOPA_{set}$ and DOPA, which could be the result of the oxidation increase as seen in Figure 3.14 compared to the more healthy control in Figure B.4 found in Appendix B.4, or that k_{22} is not administrated in doses, but in a continuous flow. This comparison is specified in the following Table 3.4. Additionally, according to Mosharov et al. levodopa is used mostly after the death of substantia nigra neurons[72], which may explain the rapid decrease in DA and DOPA, assuming that the neurons have died resulting from a too high oxidation by ROS. It may also explain the mismatch between DOPA and $DOPA_{set}$.

	Runs of a control, two of a patient		
Run	d-01	d-p1	d-p2
Tyr (μM)	762	755	755
DOPA (μM)	59.0	2.26×10^{-3}	2.12
DA (μM)	1.61	6.35×10^{-5}	6.01×10^{-2}
$DA_{vesicle}$ (μM)	12.7	1.64×10^{-2}	12.9
DA_{ext} (μM)	4.52×10^{-4}	2.06×10^{-8}	1.89×10^{-5}

TABLE 3.4: Displays the final concentrations of third phase from the runs of d-01, d-p1, and d-p2, the first being the Figure from section B.4, the second the patients values and the third with increased DOPA concentration by medication.

Looking at the values in Table 3.4, the difference between the control d-01 and d-p1 is interesting. The Tyr concentration decreases minimally, while both DOPA and DA concentrations decrease rapidly into a breakdown of them both, meaning they have not achieved robust homeostasis, it is only in the last part of third phase that they seem to stabilize. DOPA is completely broken down, even if the $DOPA_{set}$ is rapidly increasing, creating a mismatch between the two. Comparing the results of the medicated patient, d-p2, in Table 3.4 with the patient with assumed PD, d-p1, the Tyr concentrations stay exactly the same, while all other concentrations increase. This means that the medication with DOPA indeed works with the system.

However, even if the DOPA medication works to continue pushing the DA concentrations up, it does not stop ROS, k_{14}, or other oxidations of DOPA, which produce neuromelanin. According to Mosharov et al. report that more than 50% of patients would advance debilitating motor side effects, L-DOPA induced dyskinesias, by the fifth year of administration of DOPA[72]. Indicating that the results in Figure 3.15 are a temporary solution for the patient, which explains the rather low increase of DOPA and all forms of DA. This may be because the DOPA is not the regulator of itself, Greggio et al. report the synthesis of neuromelanin is shown to be driven by cytosolic DA[65]. Since DOPA cannot regulate the oxidation or its own levels, it is confirming the theory whereas DA is the regulator of DOPA.

Chapter 4

Conclusion

The collaboration of many homeostatic mechanisms, including DA auto receptors and the special properties of TH, lead to a robust dopaminergic system. The regulation of fluxes and inhibitions were confirmed against theory and finds of other studies. Moreover, the essential stability of DOPA was recognized by various conditions, were DA was strongly regulating its stability. The understanding of these homeostatic mechanisms is crucial for the design of therapeutic approaches of neurodegenerative diseases like PD. Introducing DOPA as a medication of PD, has been indicated to be effective in increasing DA levels. The computation failed to demonstrate the effect of DOPA medication of PD, because the computations were of continuous DOPA administration and not by dosages. The hope is to provide further knowledge from these studies about DA as a regulator of DOPA, but the relationship should be explored further.

Appendix A

Abbreviations used

cAMP	Cyclic Adenosine Monophosphate
DA	Dopamine
DA_{cleft}	DA in synaptic cleft
DA_{ext}	DA outside of the vesicle(s)
DA_{total}	The sum of DA, DA_{ext}, and $DA_{vesicle}$
$DA_{vesicle}$	DA inside of vesicle(s)
DDC	DOPA decarboxylase
DOPA	Dihydroxyphenylalanine
$DOPA_{set}$	Set-point of DOPA
ESRD	End-Stage Renal Disease
MAO	Methyl aluminoxane
NP	DA released by nerve pulse
6-OHDA	6-hydroxydopamine
PD	Parkinson's disease
Phe	Phenylalanine
TA	Tyramine
TH	Tyrosine hydroxylase
Tyr	L-tyrosine
TYR	Tyrosinase
ROS	Reactive Oxygen Species
VMAT-2	Vesicular Monoaminergic Transporter-2

Appendix B

The Models Before Change

The four models of *a*, *b*, *c*, and *d* are listed with the input files, graphs, and the general output from the command prompt. These models represent the cell before any changes have been made to any variable, using the values listed in Section 2.2. The input files of *b*, *c*, and *d*, are based on the input file of *a*, to make the results the most comparable.

B.1 Model *a* before change: run *a*-01

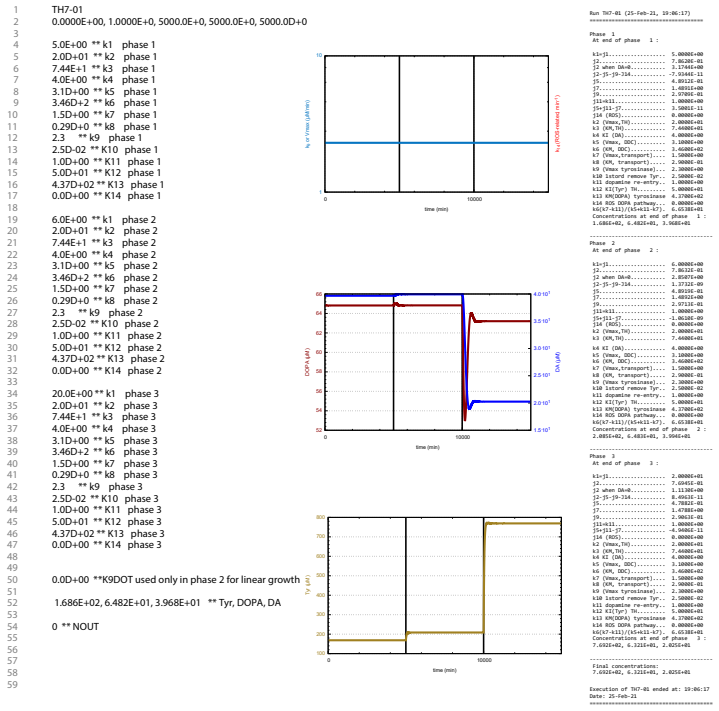

FIGURE B.1: This figure shows a run of Model a in Figure 3.1, the results are based of this run, with all constants, found in the input file to the left, remaining the same through-out the phases. The exception is of k_1, changing from 5.00μM/min in the first phase, to 6.00μM/min in the second, with 20.0μM/min in the third. In the middle, the output is shown in three graphs, the constants k_9 and k_{14} in the first graph plotted against time in minuets, DOPA and DA in the second, with Tyr concentration per min in the last graph. To the right, is the summary which show the final concentrations for Tyr, DOPA and DA, and the final output per phase for rate-constants and fluxes. The final concentrations of the second phase are the ones of interest, with 209μM for Tyr, 64.8μM for DOPA and finally 39.9μM for DA.

B.2 Model *b* before change: run *b*-01

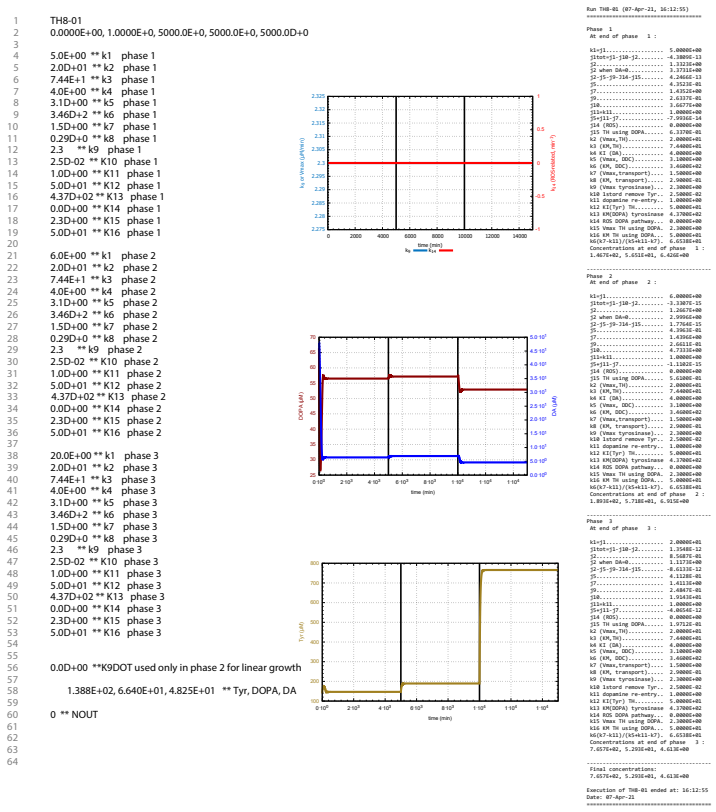

FIGURE B.2: The computation shown is the output of the model of the Model b in Figure 3.7, where the results are based of this run. This model is the same as Figure B.1 with the exception of the addition of k_{15} and k_{16}, having 2.30μM/min and 50.0μM, respectively. The final concentrations of the second phase are the ones of interest, with 189μM for Tyr, 57.2μM for DOPA and finally 6.92μM for DA.

B.3 Model *c* before change: run *c*-01

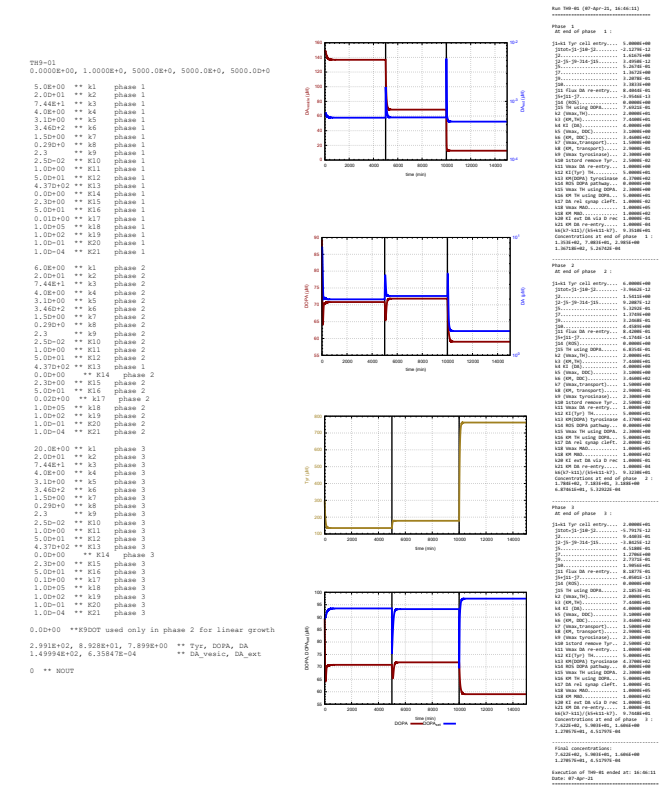

FIGURE B.3: Model c in Figure 3.10, have the results based of this run. This run is the same as Figure B.2 with the exception of an addition of k_{18}, k_{19}, k_{20} and k_{21}, which have constant values of $1.00\times10^{5}\mu$M/min, 100μM, 0.10μM and $1.00\times10^{-04}\mu$M, respectively. There is also an addition of k_{17} which has $0.01min^{-1}$ is in the first and third phase, but $0.02\ min^{-1}$ in the second. Model c has two additional graphs, whereas the graph with the constants k_9 and k_{14} has been excluded. The additional graphs show $DA_{vesicle}$ and DA_{ext} plotted against time, and the other graph show the contrast between DOPA and its set point. The final concentrations of the second phase are the ones of interest, with 189μM for Tyr, 57.2μM for DOPA and finally 6.92μM for DA, for $DA_{vesicle}$ 68.8μM, and finally $5.33\times10^{-04}\mu$M for DA_{ext}.

B.4 Model *d* before change: run *d*-01

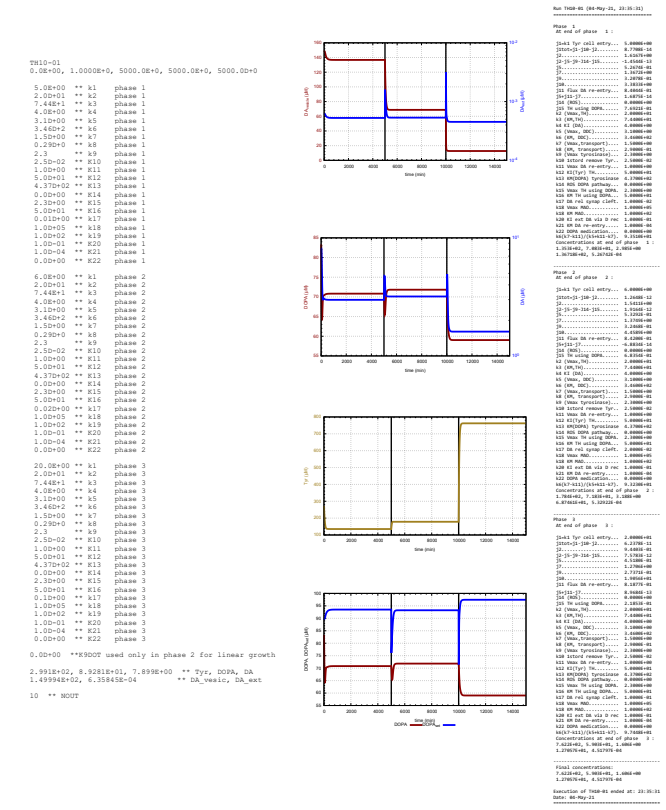

FIGURE B.4: The Model d in Figure 3.13, have the results based of this run. This run is the same as Figure B.4 except for an addition of k_{22}, which has constant value of 0μM/min, respectively. The final concentrations of the third phase are the ones of interest, with 762μM for Tyr, 59.0μM for DOPA, 1.61μM for DA, for $DA_{vesicle}$ 12.7μM, and finally $4.52\times10^{-04}\mu$M for DA_{ext}.

Bibliography

[1] Kristian Thorsen, Oleg Agafonov, Christina H Selstø, Ingunn W Jolma, Xiao Y Ni, Tormod Drengstig, and Peter Ruoff. Robust concentration and frequency control in oscillatory homeostats. *PLoS One*, 9(9):e107766, 2014.

[2] T Drengstig, K Thorsen, IW Jolma, and P Ruoff. Fysiologiske reguleringsmekanismer. *Naturen*, 137(04):128–137, 2013.

[3] Verdeil F. Robin C. Treatise of anatomical and physiological chemistry, normal and pathologic. In Langley L.L., editor, *Homeostasis: Origins of the Concept*, chapter 4, pages 77–78. Dowden, Hutchinson & Ross, Stroudsburg, Pa, 1973.

[4] Etienne Roux. The concept of function in modern physiology. *The Journal of physiology*, 592(11):2245–2249, 2014.

[5] Cannon W.B. Organization for physiological homeostasis. In L.L. Langley, editor, *Homeostasis: Origins of the Concept*, chapter 19, pages 399–431. Dowden, Hutchinson & Ross, Stroudsburg, Pa, 1973.

[6] dictionary.com. stasis, 2021 (Date accessed 25-01-2021). URL `https://www.dictionary.com/browse/stasis?s=t`.

[7] Neil A. Campbell, Lisa A. Urry, Wasserman Steven A. Cain, Michael L., and Peter V. Minorsky. *Biology; A Global Approach*, pages 934–935. Pearson, eleventh edition, 2018.

[8] David S Goldstein and Irwin J Kopin. Homeostatic systems, biocybernetics, and autonomic neuroscience. *Autonomic Neuroscience*, 208:15–28, 2017.

[9] MedlinePlus. Body temperature norms: Medlineplus medical encyclopedia, 2021 (Date accessed 25-01-2021). URL `https://medlineplus.gov/ency/article/001982.htm`.

[10] Gregory M Brown. Light, melatonin and the sleep-wake cycle. *Journal of Psychiatry and Neuroscience*, 19(5):345, 1994.

[11] Claude Bernard. *Leçons sur les phénomènes de la vie commune aux animaux et aux végétaux*, volume 2. Baillière, 1879.

[12] Marion Thomas. Charles robin et émile littré: débats sur la cellule et la continuité du vivant dans les manuels de physiologie et les cercles intellectuels parisiens dans la deuxième partie du xix e siècle. *Littèrature française et savoirs biologiques au XIXe siècle*, pages 265–280, 2019.

[13] Charles G Gross. Claude bernard and the constancy of the internal environment. *The Neuroscientist*, 4(5):380–385, 1998.

[14] Bernard C. General physiology course of the faculty of sciences, opening lecture: Introduction of the method. In Langley L.L., editor, *Homeostasis: Origins of the Concept*, chapter 5, pages 80–83. Dowden, Hutchinson & Ross, Stroudsburg, Pa, 1973.

[15] Stephen A Harwood and Sally Eaves. Homeostasis: from metaphor to mechanism in the tech – human relationship. In Kutar M. Griffiths M., McLean R., editor, *22nd UK Academy for Information Systems International Conference*, Oxford, 2017. COMMENDED PAPER; 22nd UKAIS Annual Conference, St Catherine's College Oxford, UK, 4th-5th April 2017.

[16] Suzanne Wakim and Mandeep Grewal. 21.2: Homeostasis and disease, 2021 (Date accessed 04-02-2021). URL `https://bio.libretexts.org/Bookshelves/Human_Biology/Book%3A_Human_Biology_(Wakim_and_Grewal)/21%3A_Disease/21.2%3A_Homeostasis_and_Disease`.

[17] Hiroaki Kitano. Computational systems biology. *Nature*, 420:206–210, 2002.

[18] Eberhard O Voit, Zhen Qi, and Shinichi Kikuchi. Mesoscopic models of neurotransmission as intermediates between disease simulators and tools for discovering design principles. *Pharmacopsychiatry*, 45(S 01):S22–S30, 2012.

[19] Francis Mairet. A biomolecular proportional integral controller based on feedback regulations of protein level and activity. *Royal Society Open Science*, 5(2):171966, 2018.

[20] Pramod R Somvanshi, Anilkumar K Patel, Sharad Bhartiya, and KV Venkatesh. Implementation of integral feedback control in biological systems. *Wiley Interdisciplinary Reviews: Systems Biology and Medicine*, 7(5):301–316, 2015.

[21] Larry R. Engelking. Chapter 6 - enzyme kinetics. In Larry R. Engelking, editor, *Textbook of Veterinary Physiological Chemistry (Third Edition)*, pages 32–38. Academic Press, Boston, 3 edition, 2015.

[22] Alex Yartsev. First order, zero order and non-linear elimination kinetics, 2017 (Date accessed 11-03-2021). URL https://derangedphysiology.com/main/cicm-primary-exam/required-reading/pharmacokinetics/Chapter%203.3.7/first-order-zero-order-and-non-linear-elimination-kinetics.

[23] James G Roberts, Leyda Z Lugo-Morales, Philip L Loziuk, and Leslie A Sombers. Real-time chemical measurements of dopamine release in the brain. In Humana Press, editor, *Dopamine*, volume 964, pages 275–294. Springer, 2013.

[24] Saba Khanam and Yasir H Siddique. Dopamine: agonists and neurodegenerative disorders. *Current drug targets*, 19(14):1599–1611, 2018.

[25] Iria Carballo-Carbajal, Ariadna Laguna, Jordi Romero-Giménez, Thais Cuadros, Jordi Bové, Marta Martinez-Vicente, Annabelle Parent, Marta Gonzalez-Sepulveda, Núria Peñuelas, Albert Torra, et al. Brain tyrosinase overexpression implicates age-dependent neuromelanin production in parkinson's disease pathogenesis. *Nature Communications*, 10(1):1–19, 2019.

[26] Juan Segura-Aguilar, Irmgard Paris, Patricia Muñoz, Emanuele Ferrari, Luigi Zecca, and Fabio A Zucca. Protective and toxic roles of dopamine in parkinson's disease. *Journal of Neurochemistry*, 129(6):898–915, 2014.

[27] Andrea Herrera, Patricia Munoz, Harry WM Steinbusch, and Juan Segura-Aguilar. Are dopamine oxidation metabolites involved in the loss of dopaminergic neurons in the nigrostriatal system in parkinson's disease? *ACS Chemical Neuroscience*, 8 (4):702–711, 2017.

[28] Shenyu Zhai, Weixing Shen, Steven M Graves, and D James Surmeier. Dopaminergic modulation of striatal function and parkinson's disease. *Journal of Neural Transmission*, 126(4):411–422, 2019.

[29] Jane A Driver, Giancarlo Logroscino, J Michael Gaziano, and Tobias Kurth. Incidence and remaining lifetime risk of parkinson disease in advanced age. *Neurology*, 72(5):432–438, 2009.

[30] Ahmed A Moustafa, Srinivasa Chakravarthy, Joseph R Phillips, Ankur Gupta, Szabolcs Keri, Bertalan Polner, Michael J Frank, and Marjan Jahanshahi. Motor symptoms in parkinson's disease: A unified framework. *Neuroscience & Biobehavioral Reviews*, 68:727–740, 2016.

[31] Yimei Xu, Alan H Stokes, Robert Roskoski Jr, and Kent E Vrana. Dopamine, in the presence of tyrosinase, covalently modifies and inactivates tyrosine hydroxylase. *Journal of Neuroscience Research*, 54(5):691–697, 1998.

[32] S Colette Daubner, Tiffany Le, and Shanzhi Wang. Tyrosine hydroxylase and regulation of dopamine synthesis. *Archives of Biochemistry and Biophysics*, 508(1): 1–12, 2011.

[33] Alan C Hindmarsh. Brief description of odepack—a systematized collection of ode solvers-double precision version. *Center for Applied Scientific Computing*, 50:561, 2001.

[34] Alan C Hindmarsh. Lsode and lsodi, two new initial value ordinary differential equation solvers. *ACM Signum Newsletter*, 15(4):10–11, 1980.

[35] Krishnan Radhakrishnan and Alan C Hindmarsh. Description and use of lsode, the livermore solver for ordinary differential equations. Technical Report UCRL-ID-113855, Lawrence Livermore National Lab, Livermore (CA), 1993.

[36] Mitchell A Lazar, Alexandre J Lockfeld, Roger JW Truscott, and Jack D Barchas. Tyrosine hydroxylase from bovine striatum: catalytic properties of the phosphorylated and nonphosphorylated forms of the purified enzyme. *Journal of Neurochemistry*, 39(2):409–422, 1982.

[37] Montserrat Royo, S Colette Daubner, and Paul F Fitzpatrick. Effects of mutations in tyrosine hydroxylase associated with progressive dystonia on the activity and stability of the protein. *Proteins: Structure, Function, and Bioinformatics*, 58(1): 14–21, 2005.

[38] Giri R Sura, Mauricio Lasagna, Vijay Gawandi, Gregory D Reinhart, and Paul F Fitzpatrick. Effects of ligands on the mobility of an active-site loop in tyrosine hydroxylase as monitored by fluorescence anisotropy. *Biochemistry*, 45(31):9632–9638, 2006.

[39] Antje Chang, Lisa Jeske, Sandra Ulbrich, Julia Hofmann, Julia Koblitz, Ida Schomburg, Meina Neumann-Schaal, Dieter Jahn, and Dietmar Schomburg. Brenda, the elixir core data resource in 2021: new developments and updates. *Nucleic Acids Research*, 49(D1):D498–D508, 2021.

[40] Giri R Sura, S Colette Daubner, and Paul F Fitzpatrick. Effects of phosphorylation by protein kinase a on binding of catecholamines to the human tyrosine hydroxylase isoforms. *Journal of Neurochemistry*, 90(4):970–978, 2004.

[41] Mariarita Bertoldi. Mammalian dopa decarboxylase: structure, catalytic activity and inhibition. *Archives of biochemistry and biophysics*, 546:1–7, 2014.

[42] Mariarita Bertoldi and Carla Borri Voltattorni. Multiple roles of the active site lysine of dopa decarboxylase. *Archives of biochemistry and biophysics*, 488(2):130–139, 2009.

[43] Cynthia Earles, Hollie Wayment, Mitchell Green, and James O Schenk. [45] resolution of biogenic amine transporter kinetics by rotating disk electrode voltammetry: Methodology and mechanistic interpretations. *Methods in enzymology*, 296:660–675, 1998.

[44] Trent J Volz, Glen R Hanson, and Annette E Fleckenstein. Measurement of kinetically resolved vesicular dopamine uptake and efflux using rotating disk electrode voltammetry. *Journal of neuroscience methods*, 155(1):109–115, 2006.

[45] Stefano Fogal, Marcello Carotti, Laura Giaretta, Federico Lanciai, Leonardo Nogara, Luigi Bubacco, and Elisabetta Bergantino. Human tyrosinase produced in insect cells: a landmark for the screening of new drugs addressing its activity. *Molecular biotechnology*, 57(1):45–57, 2015.

[46] Michael. Wagner. Enzyme kinetics, behavior and analysis of rapid equilibrium and steady-state enzyme systems (segel, irwin h.). *Journal of Chemical Education*, 53 (11):A472, 1976.

[47] Janet A Best, H Frederik Nijhout, and Michael C Reed. Homeostatic mechanisms in dopamine synthesis and release: a mathematical model. *Theoretical Biology and Medical Modelling*, 6(1):1–20, 2009.

[48] Hong-Yan Han, Jae-Rin Lee, Wei-An Xu, Myong-Joon Hahn, Jun-Mo Yang, and Yong-Doo Park. Effect of cl- on tyrosinase: complex inhibition kinetics and biochemical implication. *Journal of Biomolecular Structure and Dynamics*, 25(2):165–171, 2007.

[49] Jan Haavik. L-dopa is a substrate for tyrosine hydroxylase. *Journal of Neurochemistry*, 69(4):1720–1728, 1997.

[50] Yves Boirie, Robert Albright, Maureen Bigelow, and K Sreekumaran Nair. Impairment of phenylalanine conversion to tyrosine inend-stage renal disease causing tyrosine deficiency. *Kidney International*, 66(2):591–596, 2004.

[51] I-kuan Wang, Cheng-Li Lin, Yi-Ying Wu, Che-Yi Chou, Shih-Yi Lin, Jiung-Hsiun Liu, Tzung-Hai Yen, Chiu-Ching Huang, and Fung-Chang Sung. Increased risk of parkinson's disease in patients with end-stage renal disease: a retrospective cohort study. *Neuroepidemiology*, 42(4):204–210, 2014.

[52] Francjan J van Spronsen, Margreet van Rijn, Jolita Bekhof, Richard Koch, and Peter GA Smit. Phenylketonuria: tyrosine supplementation in phenylalanine-restricted diets. *The American Journal of Clinical Nutrition*, 73(2):153–157, 2001.

[53] Bernadette M Marriott et al. Tyrosine and stress: Human and animal studies. In *Food Components to Enhance Performance: An Evaluation of Potential Performance-Enhancing Food Components for Operational Rations*. National Academies Press (US), 1994.

[54] Willem G van Ginkel, Iris L Rodenburg, Cary O Harding, Carla EM Hollak, M Rebecca Heiner-Fokkema, and Francjan J van Spronsen. Long-term outcomes and practical considerations in the pharmacological management of tyrosinemia type 1. *Pediatric Drugs*, 21(6):413–426, 2019.

[55] King, Trahms, and Scott]sniderman Lisa Sniderman King, Cristine Trahms, and C Ronald Scott. Tyrosinemia type i. In M.P. Adam, H.H. Ardinger, and R.A. et al. Pagon, editors, *GeneReviews®[Internet]*. 2006 [Updated 2017 May 25].

[56] National Center for Biotechnology Information. Pubchem compound summary for cid 5610, tyramine, 2021 (Date accessed 20-04-2021). URL `https://pubchem.ncbi.nlm.nih.gov/compound/Tyramine`.

[57] Corey Burns and Ariel Kidron. Biochemistry, tyramine. *StatPearls [Internet]*, 2020.

[58] Susan McQuillan. Maois and tyramine: Foods in your diet may lead to dangerous side effects, 2021 (Date accessed 21-04-2021). URL `https://www.psycom.net/maoi-diet-tyramine`.

[59] Emily Downward. What are mao-b inhibitors?, 2020 (Date accessed 21-04-2021). URL `https://parkinsonsdisease.net/medications/mao-b-inhibitors`.

[60] The Editors of Encyclopaedia Britannica. Michaelis-menten kinetics, 2019 (Date accessed 16-04-2021). URL `https://www.britannica.com/science/Michaelis-Menten-hypothesis`.

[61] UniProt Consortium. Biophysicochemical properties, 2018 (Date accessed 16-04-2021). URL `https://www.uniprot.org/help/biophysicochemical_properties`.

[62] Huseyin Bekir Yildiz, Salim Caliskan, Musa Kamaci, Abdullah Caliskan, and Hasim Yilmaz. L-dopa synthesis catalyzed by tyrosinase immobilized in poly (ethyleneoxide) conducting polymers. *International Journal of Biological Macromolecules*, 56: 34–40, 2013.

[63] Roskoski Robert. Modulation of enzyme activity. In S.J. Enna and David B. Bylund, editors, *xPharm: The Comprehensive Pharmacology Reference*, pages 1–11. Elsevier, New York, 2007.

[64] Yong Zhi Zhou, Raid G Alany, Victor Chuang, and Jingyuan Wen. Studies of the rate constant of l-dopa oxidation and decarboxylation by hplc. *Chromatographia*, 75(11-12):597–606, 2012.

[65] Elisa Greggio, Elisabetta Bergantino, Donald Carter, Rili Ahmad, Gertrude-Emilia Costin, Vincent J Hearing, Jordi Clarimon, Andrew Singleton, Johanna Eerola, Olli Hellström, et al. Tyrosinase exacerbates dopamine toxicity but is not genetically associated with parkinson's disease. *Journal of Neurochemistry*, 93(1):246–256, 2005.

[66] David Sulzer and D James Surmeier. Neuronal vulnerability, pathogenesis, and parkinson's disease. *Movement Disorders*, 28(1):41–50, 2013.

[67] Sabah Hassain Enayah. *Evaluation of Alterations in Dopamine and Neuro-Toxicity Caused by Co-Exposure to Lead (Pb) and Polychlorinated Biphenyls (PCBs)*. PhD thesis, The University of Iowa, 2016.

[68] Jean Lud Cadet, Subramaniam Jayanthi, Michael T McCoy, Genevieve Beauvais, and Ning Sheng Cai. Dopamine d1 receptors, regulation of gene expression in the brain, and neurodegeneration. *CNS & Neurological Disorders-Drug Targets (Formerly Current Drug Targets-CNS & Neurological Disorders)*, 9(5):526–538, 2010.

[69] Philippe Huot, Martin Lévesque, and André Parent. The fate of striatal dopaminergic neurons in parkinson's disease and huntington's chorea. *Brain*, 130(1):222–232, 2007.

[70] Stanley Fahn. Does levodopa slow or hasten the rate of progression of parkinson's disease? *Journal of Neurology*, 252(4):iv37–iv42, 2005.

[71] AbbVie AS. Doseberegningsveilder. Brochure, 2017 (Date accessed 05-05-2021). URL `https://www.duodopa.no/Admin/Public/Download.aspx?file=Files%2FFiler%2FDuodopa%2FHelsepersonell%2F00%2FDoseberegningsveileder_170396.pdf`.

[72] Eugene V Mosharov, Anders Borgkvist, and David Sulzer. Presynaptic effects of levodopa and their possible role in dyskinesia. *Movement Disorders*, 30(1):45–53, 2015.